NASA CR-152481

GEOMETRIC ASSESSMENT OF IMAGE QUALITY USING DIGITAL IMAGE REGISTRATION TECHNIQUES

Glenn E. Tisdale

Westinghouse Systems Development Division

Baltimore, Maryland 21203

August 1976

Final Report

Prepared for

GODDARD SPACE FLIGHT CENTER

Greenbelt, Maryland 20771

UNCLASSIFIED

SECURITY CLASSIFICATION OF THIS PAGE *(When Data Entered)*

REPORT DOCUMENTATION PAGE		READ INSTRUCTIONS BEFORE COMPLETING FORM
1. REPORT NUMBER	2. GOVT ACCESSION NO.	3. RECIPIENT'S CATALOG NUMBER
4. TITLE *(and Subtitle)* Geometric Assessment of Image Quality Using Digital Image Registration Techniques		5. TYPE OF REPORT & PERIOD COVERED Final Report 6. PERFORMING ORG. REPORT NUMBER 76-0803
7. AUTHOR(s) Glenn E. Tisdale		8. CONTRACT OR GRANT NUMBER(.) NAS5-20947
9. PERFORMING ORGANIZATION NAME AND ADDRESS Westinghouse Defense and Electronic Systems Center Systems Development Division Baltimore, Maryland 21203		10. PROGRAM ELEMENT, PROJECT, TASK AREA & WORK UNIT NUMBERS
11. CONTROLLING OFFICE NAME AND ADDRESS		12. REPORT DATE January, 1976 13. NUMBER OF PAGES 66
14. MONITORING AGENCY NAME & ADDRESS*(if different from Controlling Office)* NASA-Goddard Space Flight Center Code 563		15. SECURITY CLASS. *(of this report)* UNCLASSIFIED 15a. DECLASSIFICATION DOWNGRADING SCHEDULE
16. DISTRIBUTION STATEMENT *(of this Report)*		
17. DISTRIBUTION STATEMENT *(of the abstract entered in Block 20, if different from Report)*		
18. SUPPLEMENTARY NOTES		
19. KEY WORDS *(Continue on reverse side if necessary and identify by block number)* Geometric Image Assessment Digital Image Registration Multispectral, Multitemporal Pattern Recognition		
20. ABSTRACT *(Continue on reverse side if necessary and identify by block number)* The objective of this program was to demonstrate the capability of Westinghouse image registration techniques to perform a geometric quality assessment of multispectral and multitemporal image pairs. Based upon LANDSAT tapes supplied by NASA-Goddard, accuracies to a small fraction of a pixel were demonstrated. Because it is insensitive to the choice of		

DD FORM 1 JAN 73 1473 EDITION OF 1 NOV 65 IS OBSOLETE

UNCLASSIFIED

SECURITY CLASSIFICATION OF THIS PAGE *(When Data Entered)*

20. ABSTRACT (Continued)

registration areas, the technique is well suited to performance in an automatic system. It may be implemented at megapixel-per-second rates using a commercial minicomputer in combination with a special-purpose digital preprocessor.

TABLE OF CONTENTS

LIST OF ILLUSTRATIONS

LIST OF TABLES

PREFACE

The objective of this program was to demonstrate the capability of the Westinghouse image registration techniques to perform a geometric quality assessment of multispectral and multitemporal image pairs. Registration measurements were performed by computer processing of images supplied by NASA-Goddard under Contract NAS5-20947. The program was conducted by the Westinghouse Systems Development Division, Baltimore, under the cognizance of Mr. Bernard Peavey of NASA-Goddard. The Westinghouse program manager was Dr. Glenn E. Tisdale. Computer programming was performed by Mr. David T. Bissell.

It was concluded that the Westinghouse techniques are capable of providing multispectral or multitemporal registration of LANDSAT imagery to accuracies of a small fraction of a pixel. They are insensitive to the choice of registration area, provided terrain detail is present. They may be implemented at megapixel-per-second rates using commercial minicomputers in combination with a special-purpose digital preprocessor.

It is recommended that implementation of the techniques as a quality control tool be initiated by conducting a brief systems analysis.

1. INTRODUCTION

The prodigious data gathering capability of the earth resources satellites offers wide application to many fields. It also provides the challenge to extract useful information with a minimum of data processing. One solution to this problem is to follow the initial assessment of a particular area with the further detection of changes only. However, change detection requires detailed registration between the original (reference) image and the more recent sample. Because of differences in spacecraft geometry and condition, these multitemporal images, although visually similar, will not precisely register. Unless the registration can be held to within a small fraction of an image element (pixel), the change detection process will generally produce errors or false alarms.

A solution to the registration problem lies in the modification of the geometry of one image so as to correspond to the other. This could be accomplished by visual comparison between corresponding well-defined image points or objects. Aside from the effort involved, this process suffers from the difficulty of defining corresponding points to within a small fraction of a pixel. A more satisfactory answer lies in the comparison of corresponding image areas using automatic correlation techniques. Improved accuracy is possible because the displacement values depend on an array of image points. Random errors inherent in the location of a single point are averaged out by the correlation process.

Conventional correlation techniques operate by comparing sample image areas on a point-by-point basis. This process has the following disadvantages:

a. Because all of the image points are involved on an equal basis, the process is inefficient from an information handling point of view. Most image points (in areas of uniform density, for example) carry little or no information. As a result, processing systems require large bandwidth and storage capability.

b. Correlation of image density values is degraded by density variations caused by ambient illumination, seasonal changes, and differences in sensor frequency (multispectral correlation).

c. Initial acquisition between images is inefficient and slow if misregistration is sizeable, or if differences exist in relative orientation and scale.

d. Individual correlation measurements provide no indication of the direction in which a match condition will be located.

As an outgrowth of a research program in pattern recognition, Westinghouse has developed digital image registration techniques that resolve the problems stated above. These techniques were applied originally to automatic target recognition tasks, where very significant differences between images must be accommodated. As a result, they operate on the global pattern of an image area, as opposed to the specific density samples.

The objective of the reported program was to investigate the feasibility of using the Westinghouse image registration techniques as a quality control tool, offering rapid assessment of the geometric comparison between image pairs. The program was initiated in 1975 by Mr. Bernard Peavey of NASA-Goddard, following the description of the techniques by Westinghouse. The goals were to demonstrate and measure registration performance on LANDSAT images supplied by NASA and to establish the feasibility of implementing the capability at megapixel-per-second rates.

The report will proceed in Section 2 with a detailed review of Westinghouse image registration techniques. The test program to measure registration performance is described in Section 3. Implementation at megapixel-per-second rates is discussed in Section 4. Finally, conclusions and recommendations are made in Section 5.

2. WESTINGHOUSE TECHNIQUES FOR IMAGE REGISTRATION

A fully automatic image registration technique should provide for initial acquisition of the match between the images as well as the precise comparison of their individual points. The initial acquisition should be possible even though the images differ in relative orientation, position, and scale. Some existing correlation techniques require close manual alignment between the images before detailed comparison is possible. The Westinghouse techniques, based on the recognition of global image patterns, provide automatic acquisition capability, as well as precise final alignment of image points. They are based on a company-sponsored development started in 1965. U. S. Patent No. 3, 748, 644, entitled "Automatic Registration of Points in Two Separate Images," was issued to Westinghouse on July 24, 1973, to cover this approach. In addition to the concepts covered in the patent, Westinghouse has developed proprietary methods for digital image processing that are incorporated in the registration operations.

Since the digital image preprocessing methods are basic to the implementation of the Westinghouse registration technique, they are described in paragraph 2. 1. In particular, this paragraph describes a method for image preprocessing that greatly reduces image data bandwidth and extracts key image information in the form of edge contours and overall statistics. Next, paragraph 2. 2 is a description of how these preprocessor outputs are used in the general case of initial acquisition between images when limited prior knowledge is available with respect to their relative orientation, position, and scale. After completion of initial acquisition, or if sufficient prior information is available to permit initial positioning, precision registration or tracking may be accomplished at high speed, using a technique described in paragraph 2. 3.

2.1 Digital Image Preprocessor

Image registration operations are accomplished by a hybrid digital image processor, consisting of a special-purpose preprocessor (to extract key image data) followed by a programmable general-purpose processor (to extract registration vectors). A description of processor hardware is contained in Section 4. In this paragraph, the operations in the special-purpose preprocessor are described. Registration operations are described in paragraphs 2.2 and 2.3.

The function of the preprocessor is to extract the features required for registration computations from the gray level image samples. These features are straight-line contours of density gradient. In effect, the preprocessor produces a line drawing of the image. At the same time, the data bandwidth is reduced by one or two orders of magnitude, depending on the selected thresholds for minimum gradient detection and line length. In addition, the preprocessor routinely extracts statistics associated with a uniform matrix of image areas. During this program, these textural statistics were used in the selection of appropriate prefilters, as discussed in paragraph 3.3.

Operation of the preprocessor is on a line-by-line basis with respect to the input image. Therefore, video data may be handled directly. Furthermore, storage requirements in the preprocessor are limited to single lines of data only. The preprocessor comprises a series of shift registers. Data flow through the line extraction portion of the preprocessor is shown in Figure 2-1.

We will demonstrate the individual preprocessor operations with the use of LANDSAT images 1703-17590 (Reel 2) and 1739-17575 (Reel 2) representing location N 36 deg, W 120 deg (near Fresno, California) on June 26, 1974, and August 1, 1974, respectively. Portions of these images (MSS Band 4) are displayed in Figure 2-2. In particular, we will concern ourselves with the windows A and A', measuring 125 x 125 pixels in size.

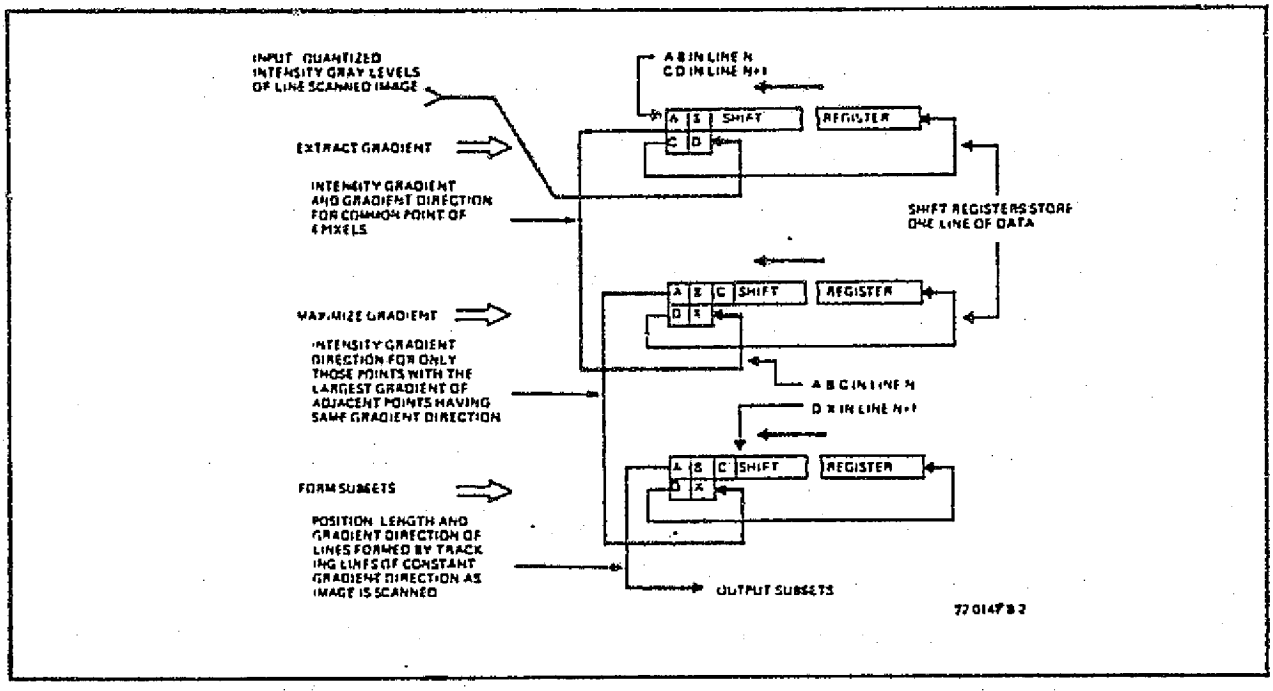

Figure 2-1. Flow of Data Through the Preprocessor

Gray level density values for these two areas are shown by Figure 2-3. The numbers represent the density to the nearest of 16 levels. Numbers above 9 are indicated with an overprinted "/". Large numbers represent dark areas.

2.1.1 Image Prefiltering

Before preprocessing the images for line extraction, spatial filtering operations may be performed on the gray level data for purposes of noise smoothing or equalization of resolution in both dimensions. It was found desirable to provide filtering between the sensor scan lines of the LANDSAT data, as explained in paragraph 3.3. Filtering between lines requires storage of one line of data samples in addition to those shown in figure 2-1.

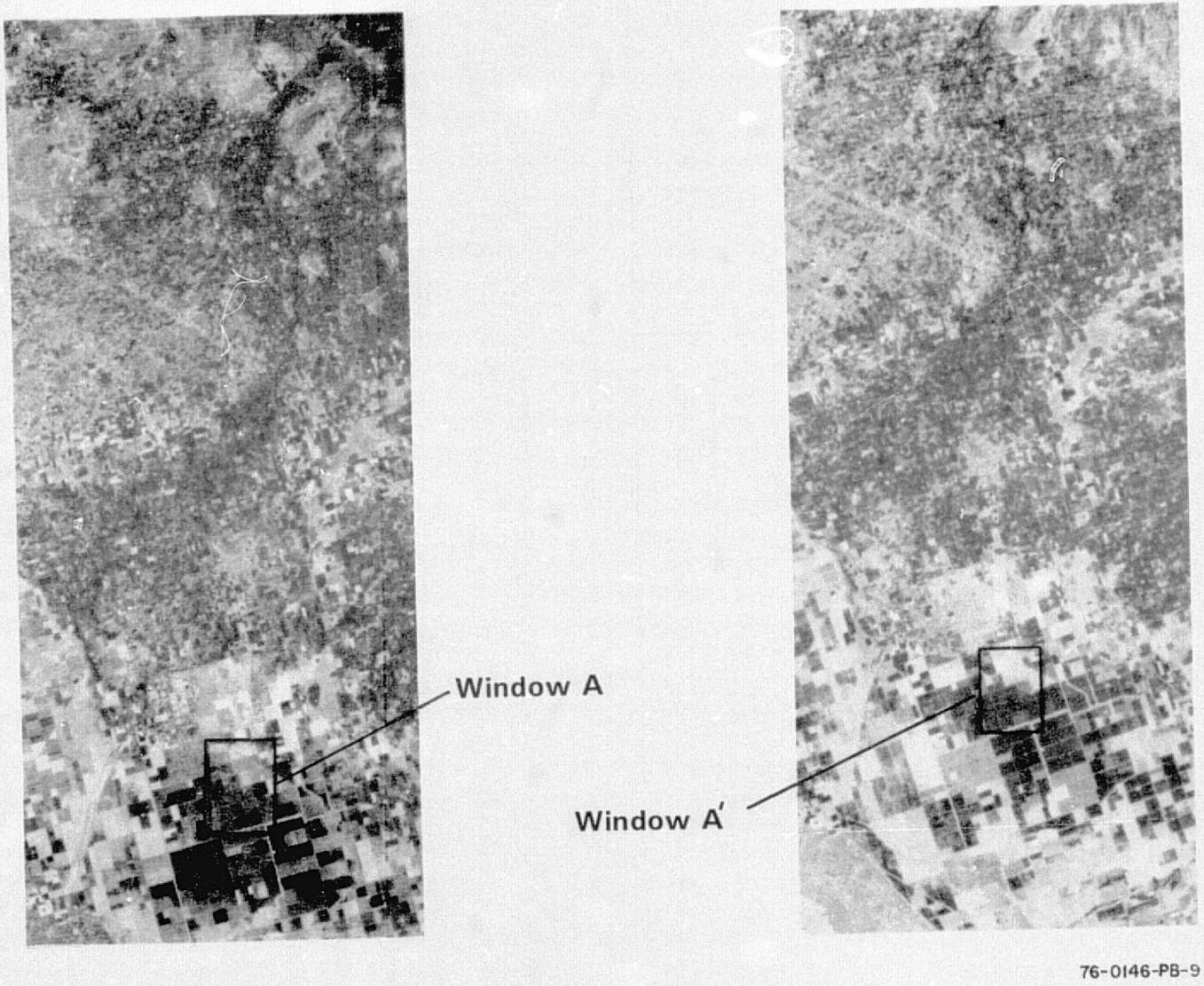

Figure 2-2. Portions of LANDSAT Images - (a) 1703-17590 and (b) 1739-17575 in the Vicinity of Fresno, California for June 26, 1974, and August 1, 1974, Respectively

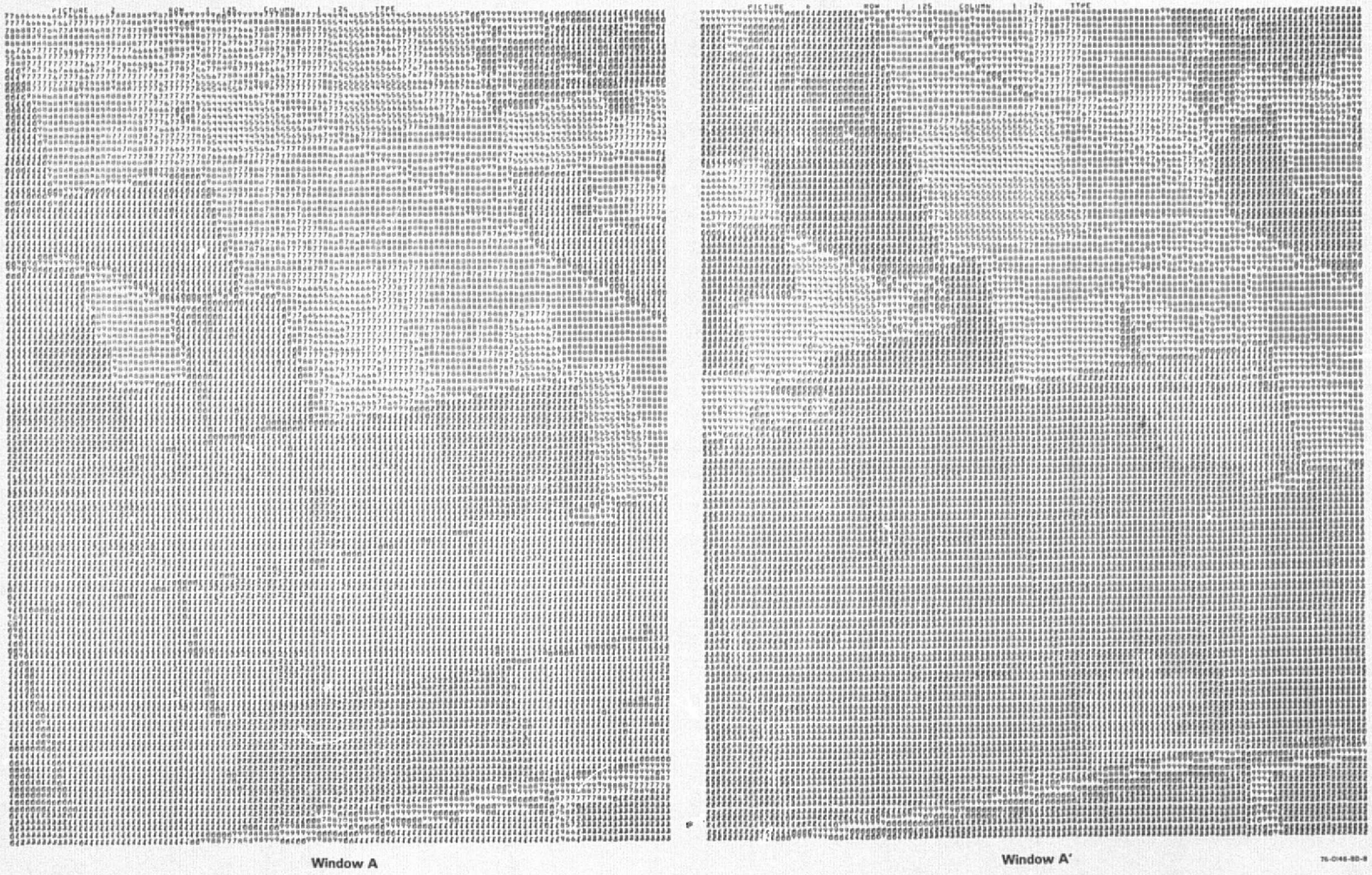

Figure 2-3. Gray Level Density Values for Windows A and A' in Figure 2-2

2.1.2 Gradient Extraction

To generate the straight-line contours (subsets) of the image, it is first necessary to compute the two-dimensional gradient (derivative) at each image point. As shown in Figure 2-4, this is done with a four-pixel window, which scans across the image in a raster format. The gradient amplitude and direction are approximated as shown. The gradient direction (0 to 360 degrees) is quantized to one of 16 discrete directions, as depicted in the diagram. To suppress the areas of negligible gradient activity (containing no significant contour or edge information), a threshold is applied to the gradient amplitude. Gradients with amplitudes less than the threshold are set at 0. A display of gradient directions for windows A and A' in Figure 2-2 is shown in Figure 2-5. The numbers indicate direction from light to dark in accordance with Figure 2-4. Numbers above 9 are overprinted with a "/".

2.1.3 Gradient Maximizing

After gradient thresholding, the edges are generally still too wide for subset generation. Therefore, a gradient thinning operation is performed that basically "skeletonizes" wide edges.

The algorithm uses a raster scanning window containing a gradient cell, X, and four of its nearest neighbors. The neighbors with colinear gradient directions are compared to X. The largest gradient amplitude is then retained. This procedure is repeated sequentially for each gradient point in the image. The maximized gradient display for images A and A' is shown by Figure 2-6; compare this with Figure 2-5.

2.1.4 Subset Generation

Subset generation is accomplished by "growing" a line formed by adjacent parallel gradients. As before, a 5-cell scanning window is employed (see Figure 2-7). The new data point is labeled cell X. Its four neighbors are examined to find those containing a parallel (within a tolerance) gradient direction. If one is found, then the neighbor is dropped as a line endpoint,

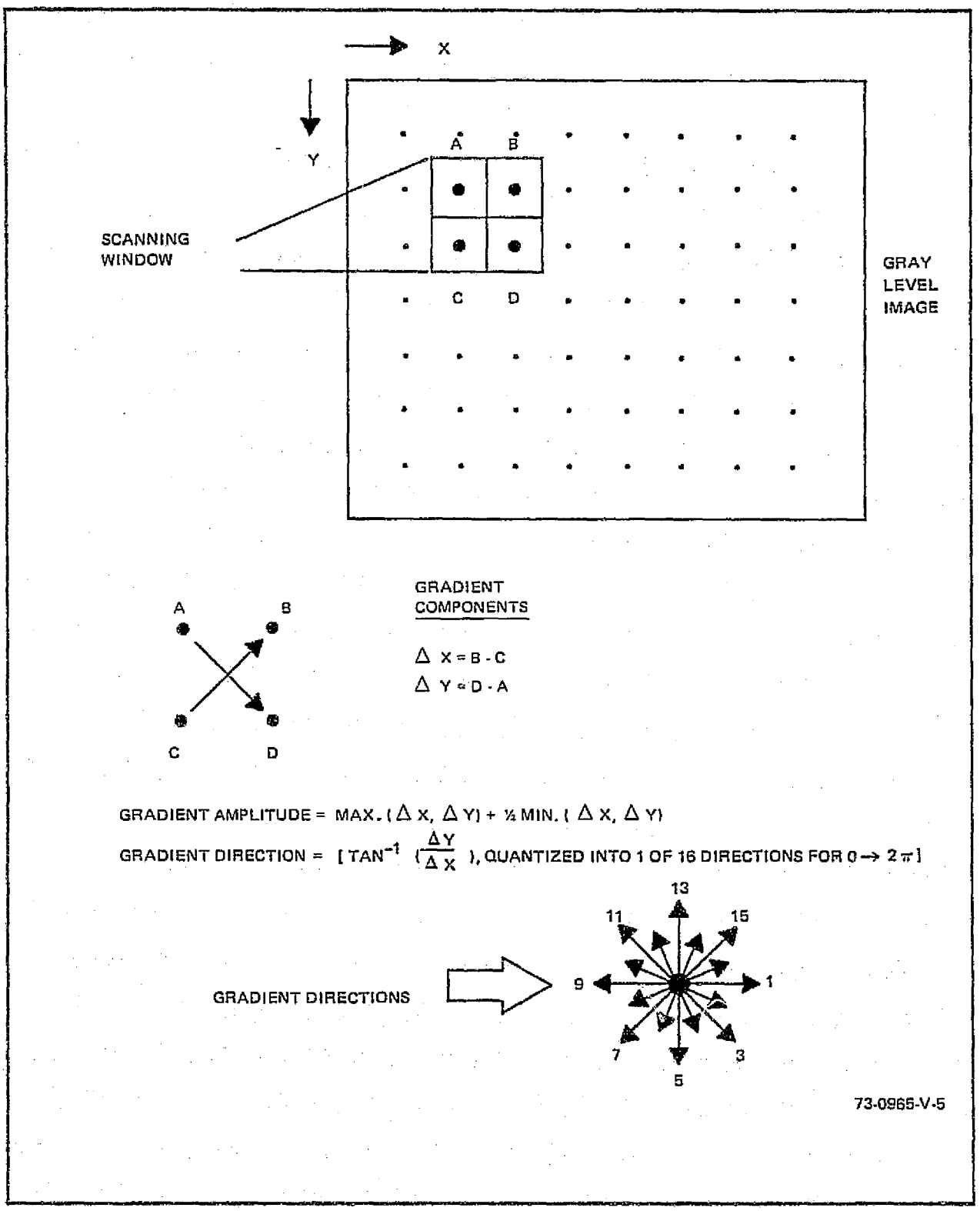

Figure 2-4. Gradient Extraction Process

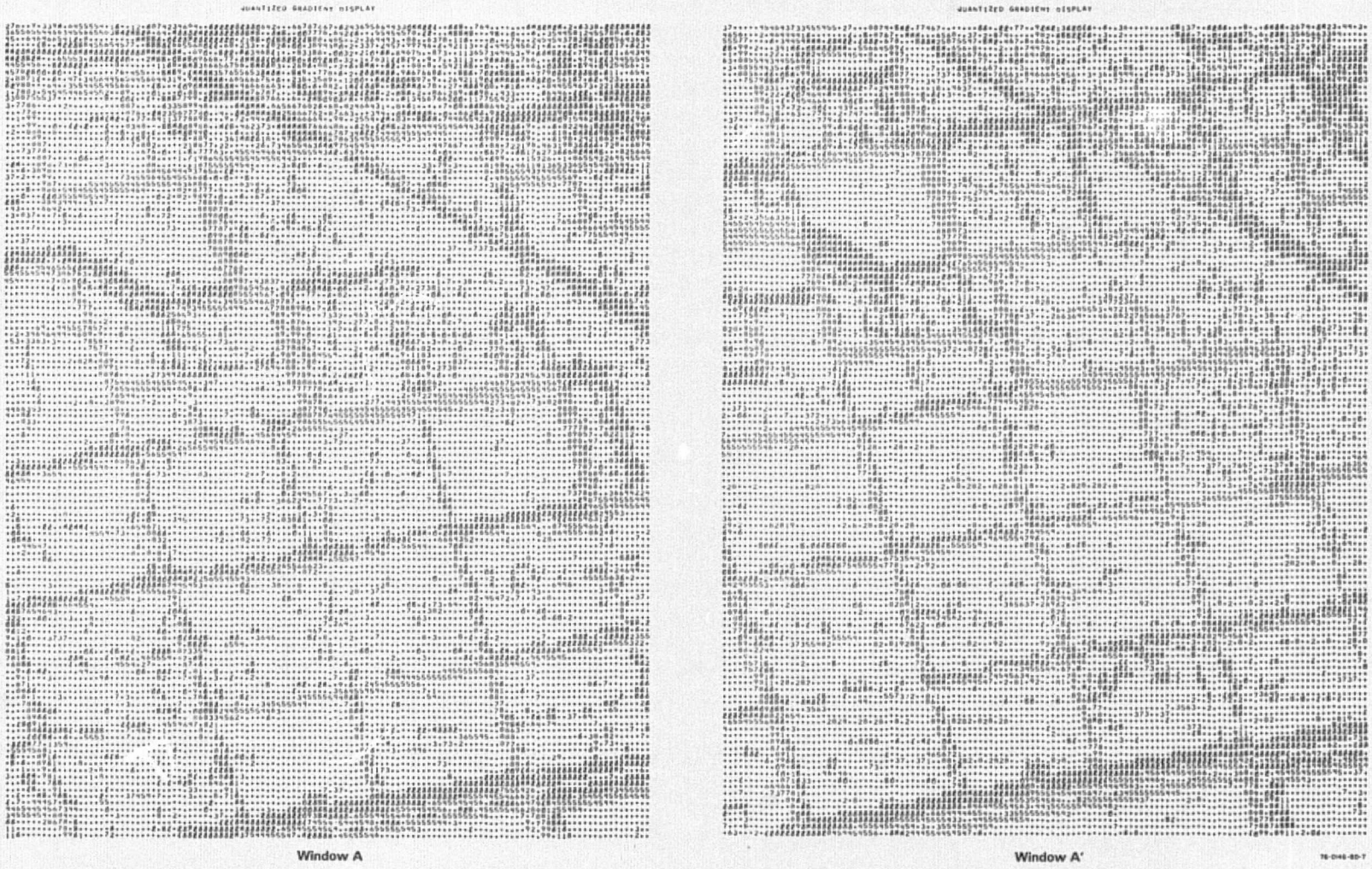

Figure 2-5. Gradient Directions for the Windows in Figure 2-2

Figure 2-6. Maximized Gradients for the Windows in Figure 2-3

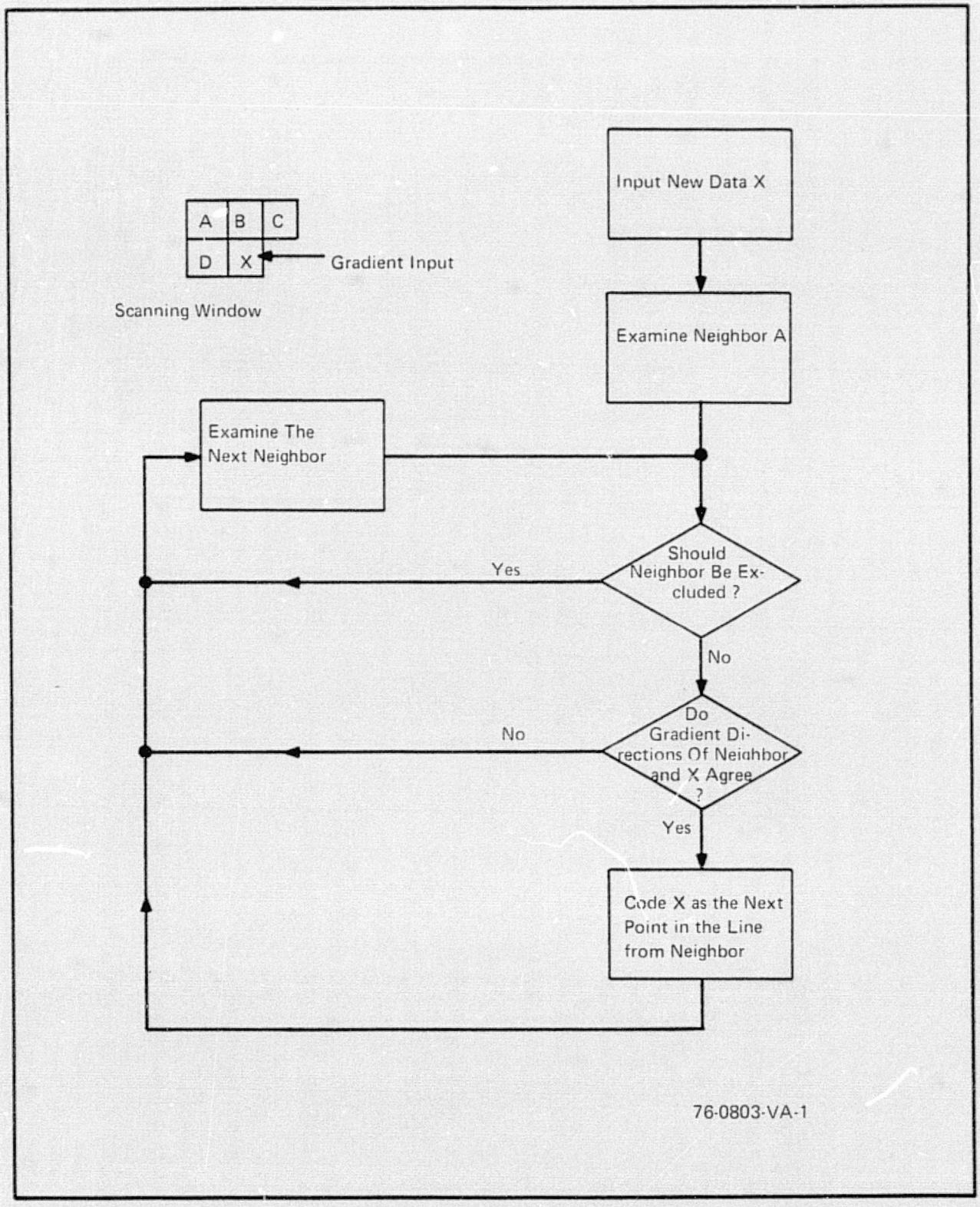

Figure 2-7. Subset Generator Operational Cycle

and X becomes the new endpoint. Neighbors that are colinear to the gradient of X are excluded to prevent false lines from forming. The operational cycle of the subset generator is diagrammed in figure 2-7.

The subsets derived from images A and A' are shown in the graphical plots in Figure 2-8. The subsets are numbered consecutively according to their lowest position on the plots. The polarity (location of light and dark sides) for each subset is coded by the presence or absence of stars at both ends. In general, the absence of the star indicates a change from light to dark in the clockwise direction, for an axis of rotation about the uppermost endpoint. For horizontal subsets, the axis of rotation is placed at the right end of the subset.

2.1.5 Texture Statistics

A second preprocessor function is the collection of statistics over a matrix of square image areas. The measurements amount to a textural analysis of the windows. They include histograms of gray density, gradient amplitude and direction, and subset length. Average values for gray density and gradient amplitude are also computed.

2.2 Initial Acquisition

The Westinghouse image processing techniques can achieve registration between two line-by-line scanned images of the same area totally independent of relative orientation and independent of position and scale over reasonable ranges. The registration output includes a measure of image similarity between the images, their relative scale and orientation, and the transformation of points between images. These steps are carried out in the sequence shown in Figure 2-9.

With reference to Figure 2-9, video signals from both images are digitized and preprocessed to extract image density contours or subsets, as described in paragraph 2.1. The subsets are defined by their endpoints. Features are formed from the subsets that consist of the geometric relationships between pairs of subsets and provide properties that are invariant, regardless of

Figure 2-8. Line Contours (Subsets) for the Windows in Figure 2-3

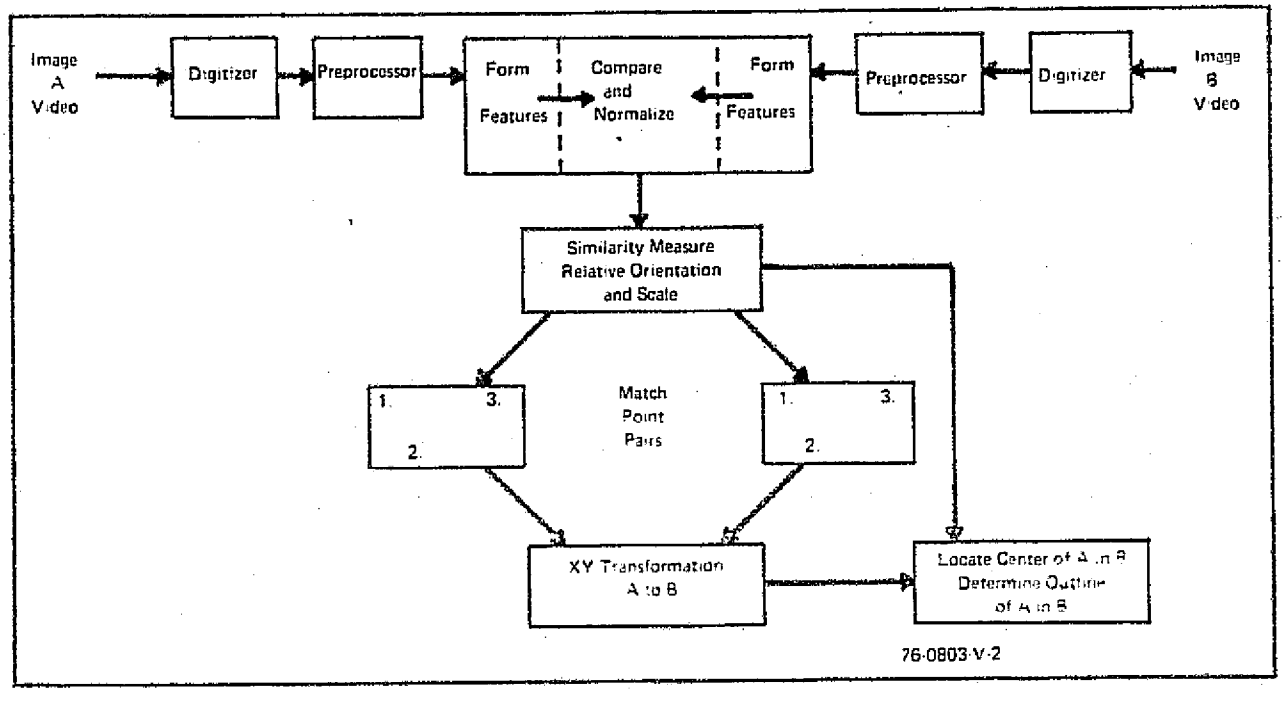

Figure 2-9. Registration Steps for Initial Acquisition

relative position, orientation, or scale. For example, these properties can include the relative angles between subsets. These features are compared between images, with the initial result being a measure of similarity associated with the registration, as well as a measure of their relative orientation and scale. When the similarity match has been accomplished, endpoints on the corresponding contours in the images can be related. In particular, the center point of one image can be located on the second image.

The computations associated with a pair of subsets are listed in Figure 2-10. Subsets AB and CD in image A correspond to A'B' and C'D' in image B. A geometric feature is formed between the pairs by connecting endpoints A and C and A' and C'. The angles between the subsets and the connecting lines, γ_1, γ_2, and γ_1' and γ_2' will be equal if figures ABDC and A'B'D'C' are similar. Furthermore, their values are invariant with translation, scale, and orientation of these figures in the plane. Accordingly, these angles are

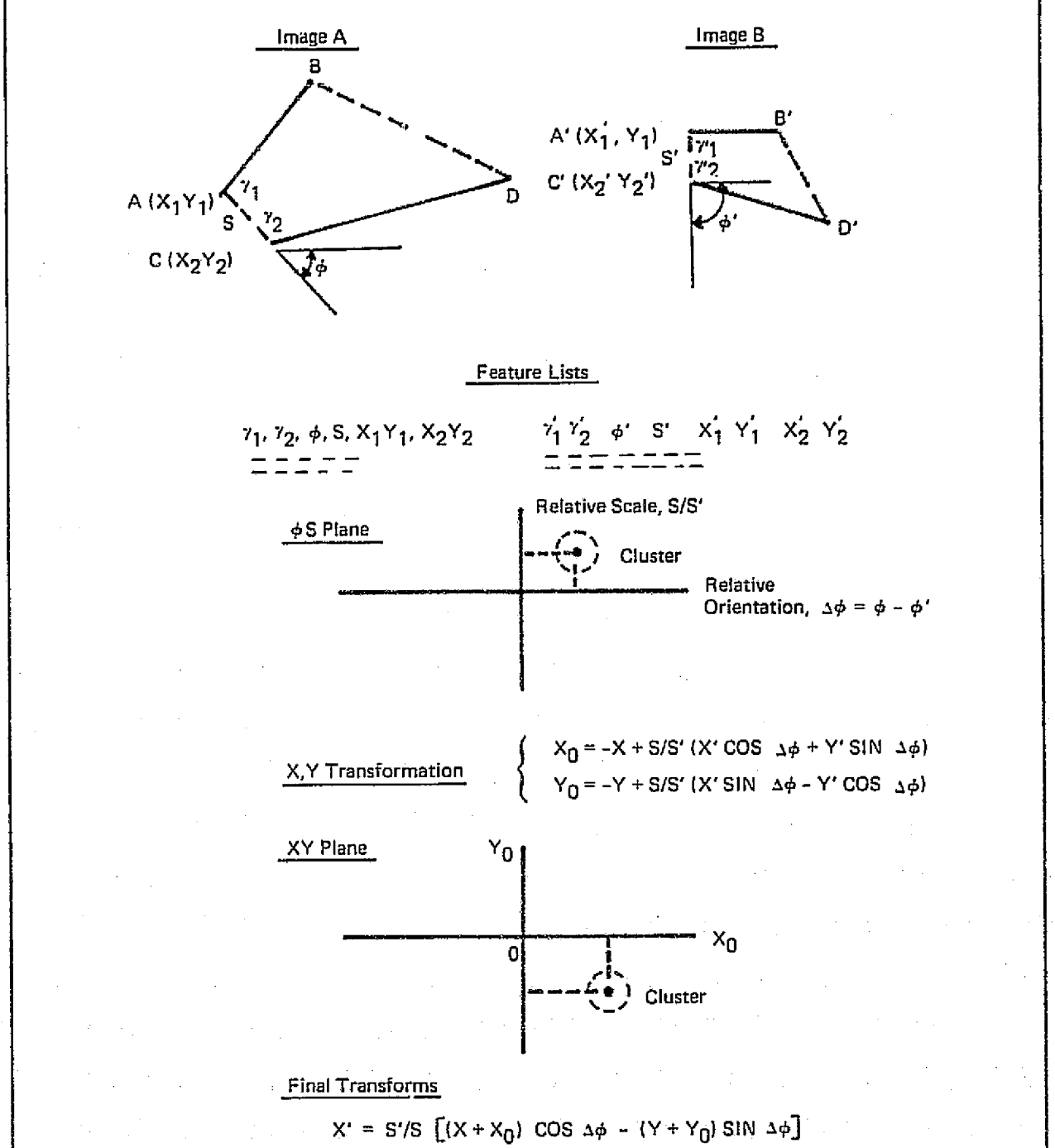

Figure 2-10. Computations in the General Case of Initial Acquisition between Images with Uncertainty of Position, Orientation, and Scale

the first elements in the geometric features used to achieve automatic acquisition. Along with these angles, the features also include the orientation, ϕ, ϕ', of the connecting lines relative to a reference axis in the image, and the lengths, S and S', of the connecting lines. They also include the subset endpoints.

Initial acquisition is obtained by matching pairs of features between the images with respect to γ, and by clustering the results with respect to relative orientation and relative scale. If the two images are identical except for translation, rotation, and scale, all the features will cluster at a point. If they have relative distortion, the cluster will be dispersed. The amount of acceptable distortion is controlled by an adjustable threshold.

The center of the cluster provides values for the relative orientation and scale of the two images. These values may be used to determine a transformation between the x and y coordinates for the two images. Since corresponding features contain endpoint coordinates, each pair can be used to calculate the nominal coordinates of translation, x_o, y_o, between the images. These are again clustered to obtain an average over the images, and to eliminate anomalies caused by symmetrical figures such as rectangles. The cluster center in the x_o, y_o plane is used with the ϕ, S values to complete the final transformation from any point in image B to the corresponding point in image A.

Where correction for image warp is desired (for example, in change detection operations), registration is carried out on a matrix of windows having sufficient density to accommodate the warp function.

If one or more parameters, such as relative scale, are known, then the process can be carried out with less computation, and with improved precision, than would otherwise be the case.

2.3 Precision Registration

The process of precision registration can begin when the initial acquisition between images has been completed, or it can be carried out directly if relative scale, orientation, and position between the images results in differences between them amounting to only a few pixels. Precision registration makes use of preprocessor subsets, as did the initial acquisition process. However, the computations are greatly simplified. In fact, a positional search, with scale and orientation known, is generally most readily accomplished by performing a matrix of precision registration measurements. These operations are demonstrated below.

The precision registration process involves the matching of corresponding subset endpoints between the two image areas and the computation of their average relative displacements by summation over the areas. With reference to Figure 2-11, windows are erected in one image around the location of subset endpoints from the other image. If subsets of appropriate direction

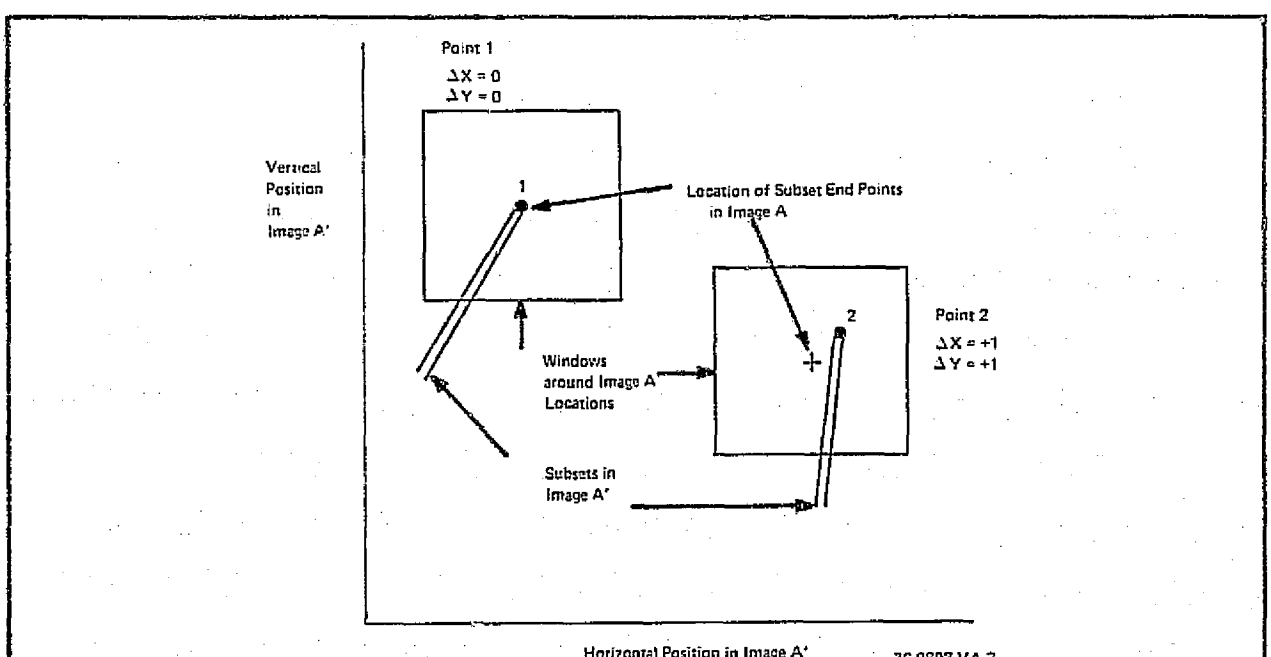

Figure 2-11. Matching of Subset Endpoints in the Precision Registration Process

terminate within the windows, the displacement of the endpoint relative to the window center is computed. For the window at upper left in Figure 2-11 (Point 1), the displacement is $\Delta x = 0$, $\Delta y = 0$. For the window at lower right (Point 2), the displacement is $\Delta x = +1$, $\Delta y = +1$.

Over the entire image area, the coordinates for the average displacement will be

$$\overline{\Delta x} = \frac{\Sigma \Delta x}{n}$$
$$\overline{\Delta y} = \frac{\Sigma \Delta y}{n} \qquad (2\text{-}1)$$

where n is the number of matching endpoints.

The registration algorithm includes a procedure for handling the occurrence in the window of more than one subset. In the event that no matching subset is found, there is no contribution to the summation.

The error in the displacement of computation of equation 2-1 depends on the positional uncertainty of the subset endpoints relative to the actual ground characteristics they represent and the number of measurements, n, over the area, as follows:

$$\text{Error} = \frac{\text{Positional Uncertainty}}{\sqrt{n}} \qquad (2\text{-}2)$$

The positional uncertainty includes the effects of noise in the sensor system, the quantizing effects of positioning to the nearest pixel, and the characteristics of the preprocessor in assigning endpoints to the subsets. The summation of these effects is expected to produce a positional uncertainty of about 2 pixels with the LANDSAT imagery, and in a random direction.

The positional uncertainty in equation 2-2 involves a pair of endpoints, one in each image. Accordingly, it is larger than the estimate for one endpoint as stated above. If we designate the positional uncertainties for the endpoints as a and b, and the angle between them as θ, then the net indicated uncertainty, u, will be given by

$$u^2 = a^2 + b^2 - 2ab \cos \theta, \qquad (2\text{-}3)$$

from simple geometry. Since the angle between them is assumed to take any value at random, the average value for the term on the right is zero. Accordingly, a good estimate for the combined positional uncertainty for a pair of endpoints is the rms value for two endpoints, or about 2.8 pixels.

If 100 endpoint pairs are involved in a displacement measurement, in accordance with equation 2-2, the expected error will be 0.28 pixel. If 400 pairs are available, the error would drop to 0.14 pixel. If 800 were available, the expected error would be 0.10 pixel. An increase in image area usually results in a corresponding increase in the number of available endpoints. Therefore, if an area of 125 pixels on each side produces a relative displacement accuracy of 0.28 pixel, an area of 350 pixels on a side should produce an accuracy of 0.10 pixel.

In Section 3, accuracy measurements are discussed that can be compared with the above estimates.

2.3.1 Computation of Relative Displacement

The characteristics of the displacement computation are readily visualized if a matrix of registration measurements is made in the vicinity of the position of best match. Such a matrix is useful for initial acquisition if relative translation is present, but orientation and scale differences are minor. However, few of these computations are ordinarily required when acquisition has been made.

A matrix of measurements for the windows A and A' of Figure 2-3 is described in Figures 2-12, 2-14, and 2-15. The matrix includes 20 relative positions in both x and y, or a total of 400 computations. The matrix of Figure 2-12 shows the number of matching endpoint pairs (divided by 100). In this computer printout, the numbers along the axes relate to the coordinates of the windows on the NASA digital tapes. The crossed lines locate the position of best match, which will be subsequently computed. The box of six pixels on a side corresponds to the size of the match window (see Figure 2-11).

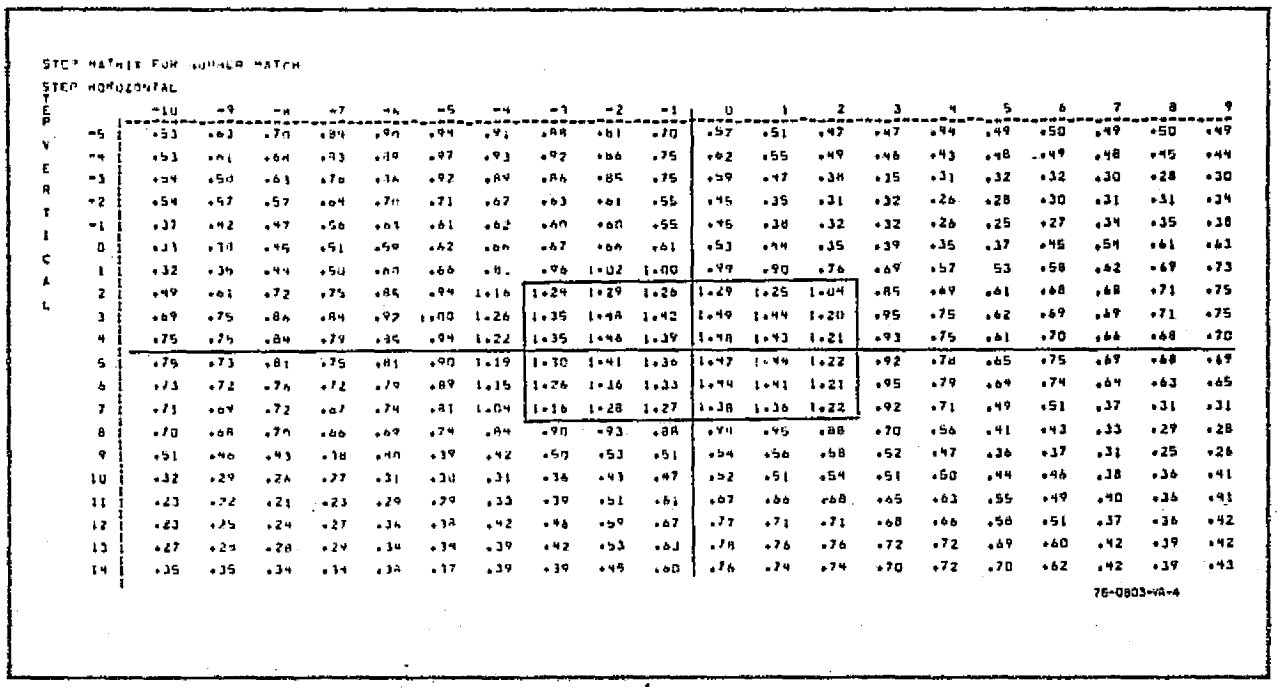

STEP MATRIX FOR DOUBLE MATCH

STEP HORIZONTAL

STEP VERTICAL	-10	-9	-8	-7	-6	-5	-4	-3	-2	-1	0	1	2	3	4	5	6	7	8	9
-5	.53	.63	.70	.84	.90	.94	.91	.88	.81	.70	.57	.51	.47	.47	.44	.49	.50	.49	.50	.49
-4	.53	.61	.64	.83	.89	.97	.93	.92	.86	.75	.62	.55	.49	.46	.43	.48	.49	.48	.45	.44
-3	.54	.60	.63	.78	.84	.92	.89	.86	.85	.75	.59	.47	.38	.35	.31	.32	.32	.30	.28	.30
-2	.54	.57	.57	.64	.70	.71	.67	.63	.61	.56	.45	.35	.31	.32	.26	.28	.30	.31	.31	.34
-1	.37	.42	.47	.56	.61	.61	.62	.60	.60	.55	.46	.38	.32	.32	.26	.25	.27	.34	.35	.38
0	.31	.38	.46	.51	.59	.62	.66	.67	.66	.61	.53	.44	.35	.39	.35	.37	.46	.54	.61	.63
1	.32	.36	.44	.50	.60	.66	.8.	.96	1.02	1.00	.99	.90	.76	.69	.57	53	.58	.62	.69	.73
2	.49	.61	.72	.75	.85	.94	1.16	1.29	1.29	1.26	1.29	1.25	1.04	.85	.69	.61	.68	.68	.71	.75
3	.69	.75	.86	.84	.92	1.00	1.26	1.35	1.48	1.42	1.49	1.44	1.20	.95	.75	.62	.69	.69	.71	.75
4	.75	.75	.84	.79	.86	.94	1.22	1.35	1.46	1.39	1.48	1.43	1.21	.93	.75	.61	.70	.66	.68	.70
5	.76	.73	.81	.75	.81	.90	1.19	1.30	1.41	1.36	1.47	1.44	1.22	.92	.74	.65	.75	.69	.68	.69
6	.73	.72	.76	.72	.79	.89	1.15	1.26	1.36	1.33	1.44	1.41	1.21	.95	.79	.69	.74	.64	.63	.65
7	.71	.69	.72	.67	.74	.81	1.04	1.16	1.28	1.27	1.38	1.36	1.22	.92	.71	.49	.51	.37	.31	.31
8	.70	.68	.70	.66	.69	.74	.84	.90	.93	.88	.90	.95	.88	.70	.56	.41	.43	.33	.29	.28
9	.51	.46	.43	.38	.40	.39	.42	.60	.53	.51	.54	.56	.58	.52	.47	.36	.37	.31	.25	.26
10	.32	.29	.28	.27	.31	.30	.31	.36	.43	.47	.52	.51	.54	.51	.60	.44	.46	.38	.36	.41
11	.23	.22	.21	.23	.29	.29	.33	.39	.51	.61	.67	.66	.68	.65	.63	.55	.49	.40	.36	.43
12	.23	.25	.24	.27	.34	.38	.42	.48	.59	.67	.77	.71	.71	.68	.66	.58	.51	.37	.36	.42
13	.27	.28	.28	.29	.34	.39	.39	.42	.53	.63	.78	.76	.76	.72	.72	.69	.60	.42	.39	.42
14	.35	.35	.34	.34	.38	.37	.39	.39	.48	.60	.76	.74	.74	.70	.72	.70	.62	.42	.39	.43

76-0803-WA-4

Figure 2-12. Matrix of the Number of Matching Subset Endpoints (÷100) for Windows A and A' of Figure 2-3

Note that in the vicinity of the best match position, the number of matching pairs rises well above surrounding values. The increased values indicate an increased correlation for these locations. Values for best match represent approximately one-third the available subset endpoints.

Some matches will generally occur for any relative position between the images. The actual number will depend on the size of the match window, the density of subset endpoints, and the specific algorithm for match acceptance. In general, a compromise will be required to balance an adequate level of matches to provide for accuracy, with a limited number of random pairings.

To appreciate the method for computation of the match position, it is useful to visualize the effect on the offset computations of sliding one set of endpoints relative to the other. In Figure 2-13, this effect is shown for one axis. A match window of 6 pixels in width is assumed (seven match positions).

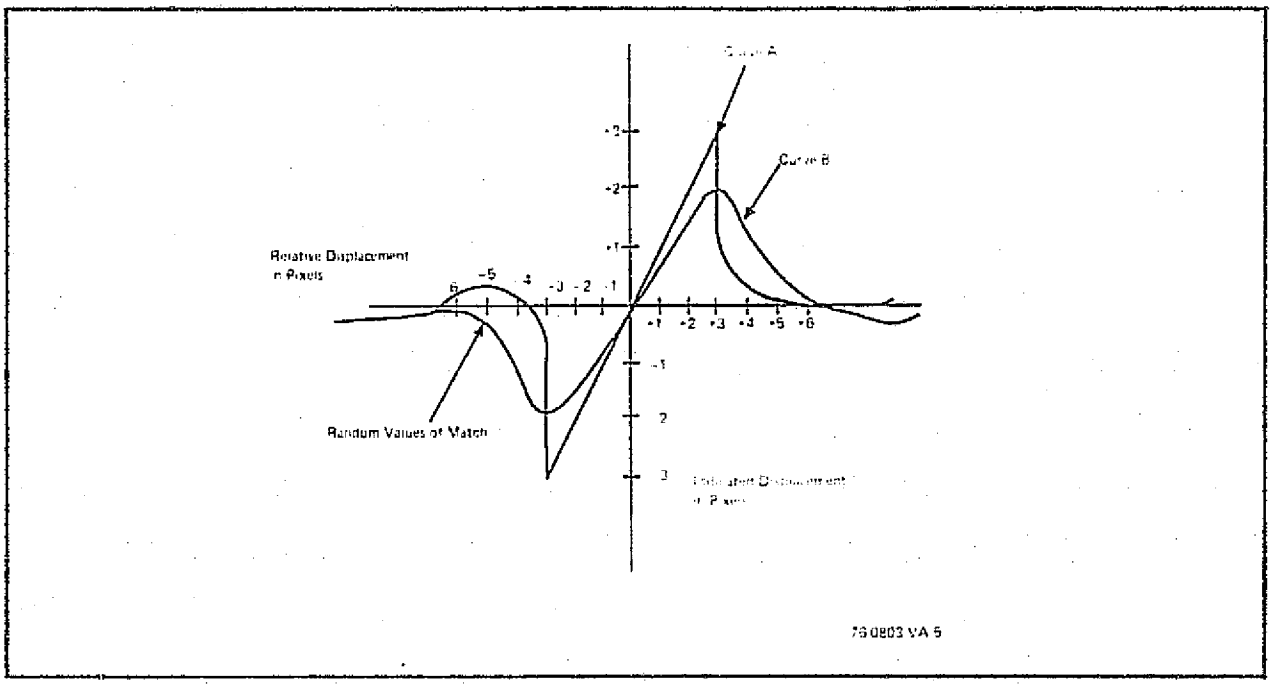

Figure 2-13. Indicated Displacement Between Images as a Function of Relative Displacement for a Single Image (Curve A) and Separate Images (Curve B) of the Same Area

The effect of sliding one image against itself is shown as Curve A. For this curve, random matches will occur until the relative displacement is equivalent to -3 pixels, at which point a match would be found between all endpoints but with an indicated displacement of -3 pixels. For the next 6 pixel positions, a linear curve of displacement would be described, as shown. When the relative displacement becomes +4, however, the output would again be the result of random matches.

For different images of the same area, a result similar to Curve B would be obtained. The values for indicated displacement are reduced by the positional uncertainty of the endpoints in each image. At the edges of the window, for example, this uncertainty will result in the loss of some matching pairs, while indicated displacement for others will appear at low values.

Calculation of the relative displacement under these conditions is carried out by a determination of the point of crossing the relative displacement axis. This is obtained by linear interpolation between the nearest integral positions.

Returning to images A and A', Figure 2-14 provides a matrix of values for the indicated displacement in the x direction (along the sensor scan lines). The corresponding displacement in the y direction is given by Figure 2-15. In Figure 2-16, the indicated displacement versus relative displacement from Figure 2-14 are plotted for both the vertical positions of 4 and 5. The similarity is obvious. Computation of the crossover point by linear interpolation would yield:

$$\Delta x_4 = \frac{0.30}{0.30 + 0.15} = 0.67$$

$$\Delta x_5 = \frac{0.36}{0.36 + 0.16} = 0.69 \qquad (2\text{-}4)$$

STEP MATRIX FOR MEAN OFF=2

STEP HORIZONTAL

STEP VERTICAL	-10	-9	-8	-7	-6	-5	-4	-3	-2	-1	0	1	2	3	4	5	6	7	8	9
-5	-.90	-.79	-.91	-.75	-.51	-.27	.19	.46	.89	.96	.93	.27	-.11	.06	.00	.02	-.09	-.04	-.90	-.12
-4	-.92	-.23	-.97	-.86	-.64	-.32	.09	.40	.81	.93	.90	.42	.00	.09	.07	.06	-.02	-.06	-.24	-.05
-3	-.35	.05	-.14	-.74	-.69	-.40	-.11	.21	.73	1.05	.81	.66	.58	.31	.29	.06	.19	-.03	-.25	.13
-2	-.39	.07	.09	-.31	-.23	-.13	-.01	.11	.52	1.00	.78	.74	.74	.19	.00	-.29	.00	-.35	-.03	.29
-1	-.76	-.48	-.16	-.34	-.19	-.33	-.11	-.03	.32	.82	.78	.79	.76	.16	-.04	.00	.19	-.59	-.49	-.05
0	-.70	-.42	-.14	-.49	-.28	-.62	-.26	-.15	.23	.66	.70	.95	.86	.05	-.66	-.41	-.51	-.80	-.51	.19
1	-.03	-.49	-.28	-.54	-.47	-.80	-.67	-.73	-.37	.14	.46	.73	1.16	.65	-.05	.06	-.21	.74	-.41	.19
2	-1.04	-.84	-.61	-.43	-.08	-.29	-.58	-.65	-.60	-.10	.29	.76	1.26	.96	.36	.30	-.09	-.78	-.49	.23
3	-.96	-.60	-.52	-.30	.07	-.20	-.50	-.68	-.67	-.22	.23	.75	1.26	1.07	.45	.24	-.12	-.68	-.46	.27
4	.06	-.37	-.49	-.72	.16	-.22	-.62	-.69	-.71	-.30	.15	.71	1.25	1.13	.48	.33	-.14	-.65	-.40	.40
5	.19	-.45	-.64	-.16	.27	-.23	-.70	-.70	-.76	-.36	.16	.67	1.20	1.10	.47	.32	-.20	-.49	-.40	.35
6	.23	-.49	-.60	-.11	.16	-.21	-.63	-.67	-.83	-.36	.10	.60	1.16	1.07	.53	.30	-.22	-.38	-.24	.43
7	.25	-.51	-.53	-.10	.15	-.06	-.56	-.71	-.99	-.51	.01	.54	1.12	1.36	1.08	.94	.61	.19	.06	.39
8	.26	-.50	-.60	-.29	.29	.26	-.04	-.33	-.66	-.54	.00	.51	.98	1.34	1.11	.68	.05	-.08	.03	.18
9	.90	.00	-.19	-.34	.13	.10	.17	-.20	-.98	-.92	-.35	-.04	.62	1.21	.87	.25	-.19	.19	.52	.27
10	.97	-.41	-.35	-.52	-.19	.03	.23	.06	-1.07	-.74	-.60	-.55	.26	.96	.94	.18	-.46	-.37	-.14	-.12
11	.65	-.36	-.19	-.74	-.64	-.39	-.21	-.19	-1.04	-.85	-.66	-.59	.21	.86	1.10	.64	.08	-.05	-.17	-.15
12	.30	-.16	-.17	-.89	-1.06	-.55	-.21	-.02	-.73	-.52	-.61	-.63	.17	.84	1.15	.66	.39	-.11	-.22	-.10
13	.03	.21	.25	-.48	-.69	-.44	-.26	-.02	-.77	-.71	-.91	-.72	-.03	.61	.94	.61	.63	.02	-.10	-.05
14	.26	.26	.54	-.15	-.58	-.24	-.33	-.05	-.67	-.55	-.93	-.86	-.15	.47	.88	.71	.61	.02	-.28	-.12

76-0803-YA-6

Figure 2-14. Matrix for Indicated Displacement in the x Direction for Windows A and A' in Figure 2-3

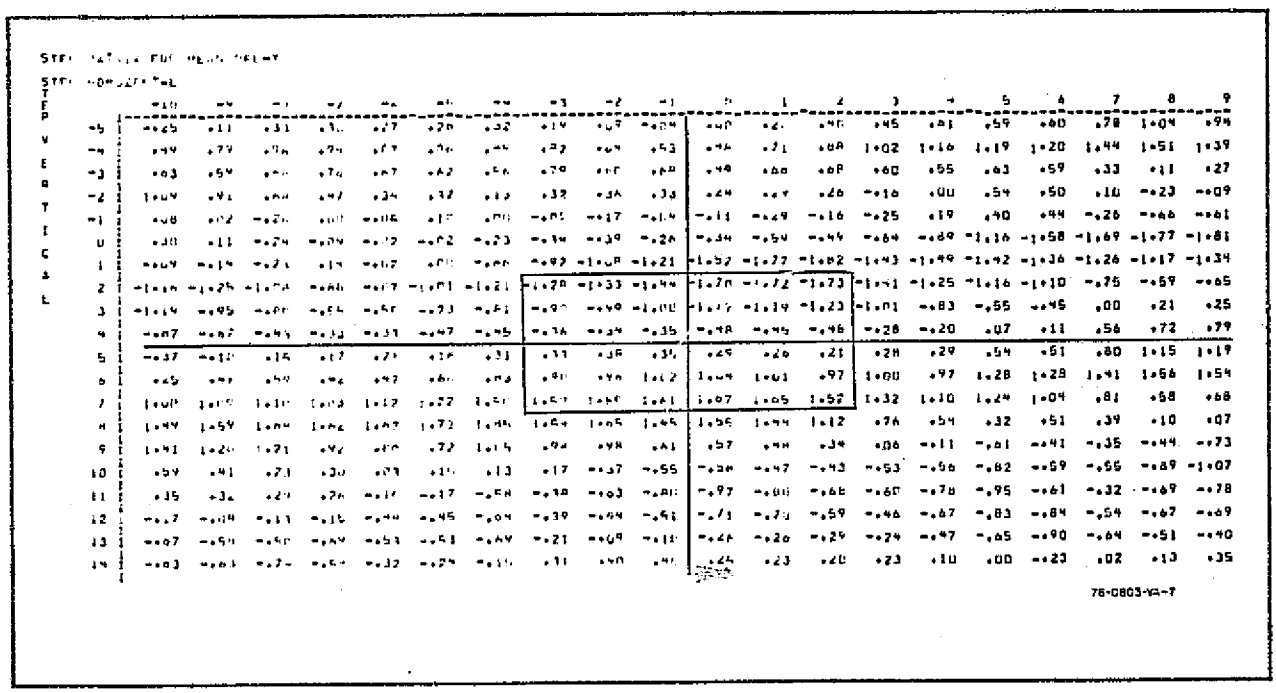

Figure 2-15. Matrix for Indicated Displacement in the y Direction for Windows A and A' in Figure 2-3

An average for these two values is 0.68. Since we are interested in performing registrations at high speed, computation of displacement was carried out for the present tests by using for both x and y the values for indicated displacement which are increased in x and y by one unit. Under these conditions, the computation for Δx would become

$$\Delta x_{45} = \frac{0.30}{0.30 + 0.16} = 0.65 \qquad (2\text{-}5)$$

This value differs from the average from equation 2-4 by 0.03 pixel. Since the number of matches (140) would indicate a positional accuracy of 0.24 pixel, the difference seems acceptable.

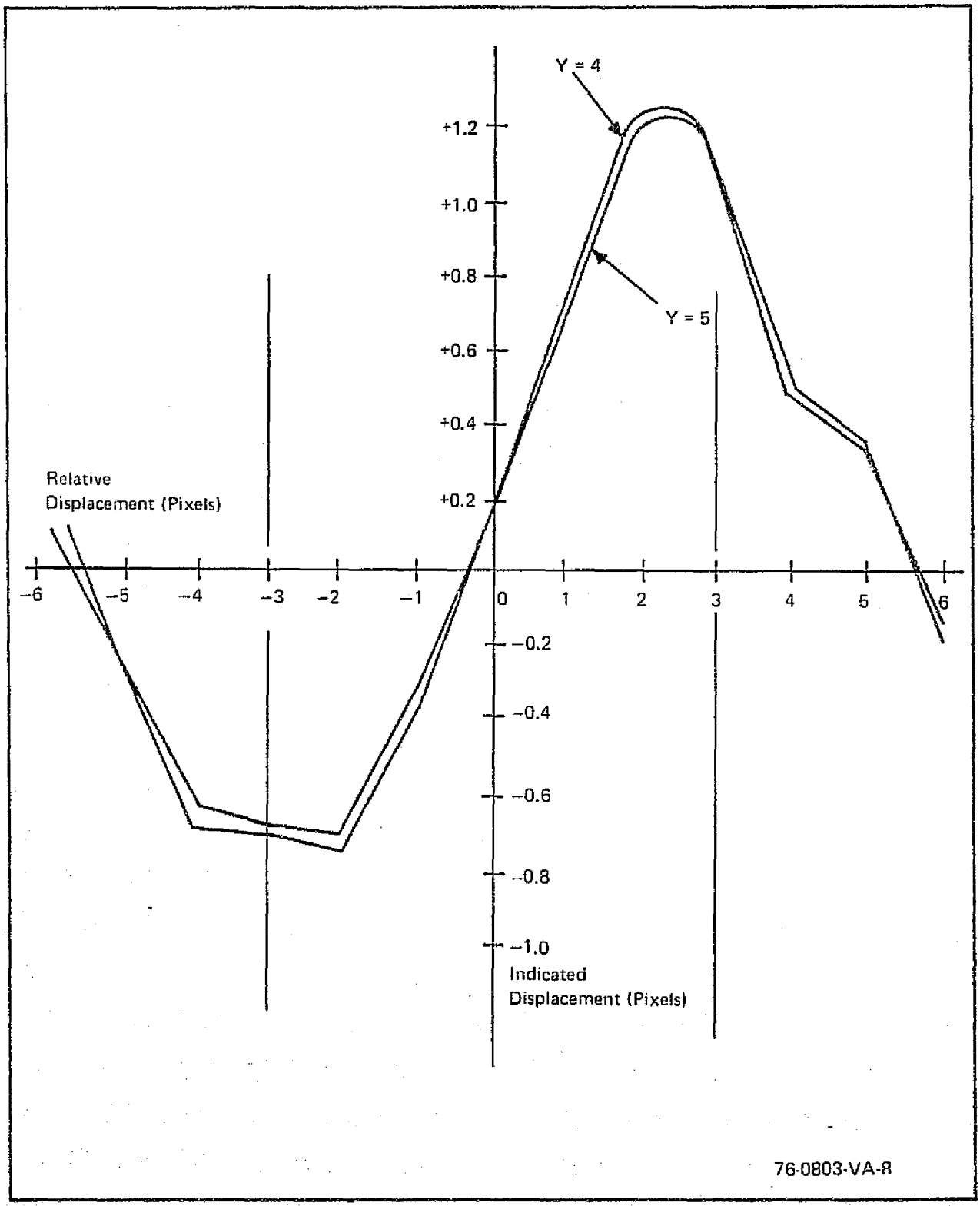

Figure 2-16. Indicated Displacement vs Relative Displacement in the x Direction for Windows A and A' in Figure 2-3

In the y direction the figures are extracted from Figure 2-15 in the downward direction for horizontal positions -1 and 0. We have

$$\Delta y_1 = \frac{0.35}{0.35 + 0.35} = 0.50$$

$$\Delta y_0 = \frac{0.48}{0.48 + 0.29} = 0.63 \qquad (2\text{-}6)$$

$$\overline{\Delta y_1 + \Delta y_0} = 0.57$$

$$\Delta y_{-1,0} = \frac{0.35}{0.35 + 0.29} = 0.55$$

The difference is 0.02 pixel in the y direction.

In the test program described in Section 3, displacements were computed by linear interpolation across diagonal positions.

3. TEST PROGRAM

The objective of the test program conducted for this study was to establish the feasibility of the Westinghouse image registration techniques to register LANDSAT imagery, both multispectral and multitemporal, and to estimate the accuracy with which this could be accomplished. The following tests were completed:

a. Multispectral registration between all combinations of the four MSS bands

b. Determination of an appropriate prefilter for the preprocessor and selection of preprocessor thresholds

c. Measurement of a distortion matrix between bulk multitemporal images

d. Measurement of a distortion matrix between previously processed and corrected multitemporal images

e. Quality measurements on specially processed multitemporal samples.

Paragraph 3.1 is a description of the methods for preparing and formatting NASA digital tapes. The tests listed above are described in paragraphs 3.2 to 3.6. An estimate of registration accuracy is computed in paragraph 3.7 from the data collected in the individual tests.

3.1 Preparation of Test Data

All image data used in performing registration measurements were obtained from NASA-Goddard on computer-compatible magnetic tapes.* They were processed at Westinghouse on a Univac 1110 system.

*Tape formats are described in NASA-GSFC Report X-563-73-206, "Generation and Physical Characteristics of the ERTS MSS System Corrected Computer Compatible Tapes," by Valerie L. Thomas, July 1973.

The first step in data preparation is to copy the tapes from 9-track 800-bpi format to the 1110 system standard of 9-track 1600-bpi. Copying the tapes provides a dump of the header identification and annotation records, but it does not separate the four image bands.

The next step is to extract windows of 125 by 125 pixels each at desired locations and to separate the four spectral bands. The choice of 125 by 125 pixels provides sufficient image area to verify registration measurements, but with low individual processing times. However, other sizes may be selected if desired. Where a uniform matrix of windows is desired, these may be extracted automatically by the extraction program. The output of the program is a magnetic tape containing a sequence of four windows for each of the four spectral bands at the desired locations. The density values for each image sample are complemented and reduced to six bits of resolution for input to the registration logic.

3.2 Multispectral Registration

In testing a registration method, the measured performance must be compared with some reliable standard, or ground truth. The ground truth may be obtained from

a. An exact knowledge of sensor geometry

b. An alternate, more reliable means for performing the measurements

c. By averaging a series of unrelated measurements at the same points.

The positioning accuracy and linearity of the LANDSAT images preclude the reliance on sensor geometry for images taken at different times (multitemporal). However, the images from the four MSS spectral bands for the same location are presumably in precise registration. Accordingly, initial testing consisted of the computation of the six multispectral combinations of these bands. The results are displayed in Table 3-1. Three scenes, each 125 by 125 pixels in size, were chosen from ERTS-E-1757-17574, located on the California coast at longitude 120 deg W, and latitude N 34 deg 30 min.

TABLE 3-1

REGISTRATION MEASUREMENTS FOR MULTISPECTRAL IMAGES

Scene	Bands	Value at 0		Adjacent Point		Relative Displacement Components		Value of Displacement	Matches	Subsets
		X	Y	X	Y	X	Y			
1	1/2	-0.14	+0.08	+0.50	-0.74	+0.28	-0.11	0.30	90	60/190
	1/3	+0.06	-0.39	-0.76	+0.51	-0.07	+0.43	0.44	71	60/221
	1/4	-0.65	-0.08	+0.32	-0.92	+0.65	+0.08	0.66	26	60/49
	2/3	+0.09	+0.01	-0.77	-0.68	-0.10	-0.01	0.10	159	190/221
	2/4	+0.20	+0.54	+0.57	+0.30	+0.26	+0.64	0.69	50	190/49
	3/4	-0.19	+0.04	+0.48	-0.53	+0.28	-0.07	0.32	85	221/49
2	1/2	-0.16	-0.04	+0.54	+0.83	+0.23	+0.05	0.24	234	168/274
	1/3	-0.15	+0.16	+0.51	-0.79	+0.23	-0.17	0.29	185	168/325
	1/4	+0.06	+0.10	-0.43	-0.73	-0.12	-0.12	0.17	72	168/184
	2/3	+0.11	-0.05	-0.41	+0.64	-0.20	+0.07	0.21	243	274/325
	2/4	+0.24	+0.06	-0.06	-0.34	-0.75	-0.14	0.76	89	274/184
	3/4	-0.12	+0.04	+0.74	-0.72	+0.14	-0.05	0.15	243	325/184
3	1/2	-0.04	+0.02	+0.95	-0.81	+0.04	-0.02	0.04	246	166/196
	1/3	-0.07	+0.09	+0.48	-0.65	+0.13	-0.12	0.18	57	166/175
	1/4	No Lock		No Lock		No Lock		--	19	166/143
	2/3	+0.23	-0.05	-0.39	+0.34	-0.37	+0.13	0.39	65	196/175
	2/4	No Lock		No Lock		No Lock		--	23	196/143
	3/4	-0.18	+0.01	+0.55	-0.01	+0.25	-0.01	0.25	161	175/143

76-0803-T-9

Scene 1 is a mountainous area, while scenes 2 and 3 are urban in nature. In all tests, the x coordinate is taken along the MSS scan (east-west), while the y coordinate is between scans (north-south).

Displacement components in Table 3-1 were calculated in the manner described in paragraph 2-3. For these multispectral samples, the values at the x = 0, y = 0 position in the displacement matrix should be 0. Actual values are tabulated in the third column of the table. A crossover point is obtained by selecting the adjacent diagonal indicated displacement value, which exhibits a change in the sign of both components, and by performing a linear interpolation. The resulting relative displacement components are shown in the fifth column. The amplitude of this displacement is also tabulated, together with the number of endpoint matches, and the number of subsets in the images from which the matches are obtained.

It is of interest to plot the error as a function of the number of matches in the window. The displacement values of Table 3-1 are located in Figure 3-1 in this manner, with the pair of spectral bands indicated beside each point.

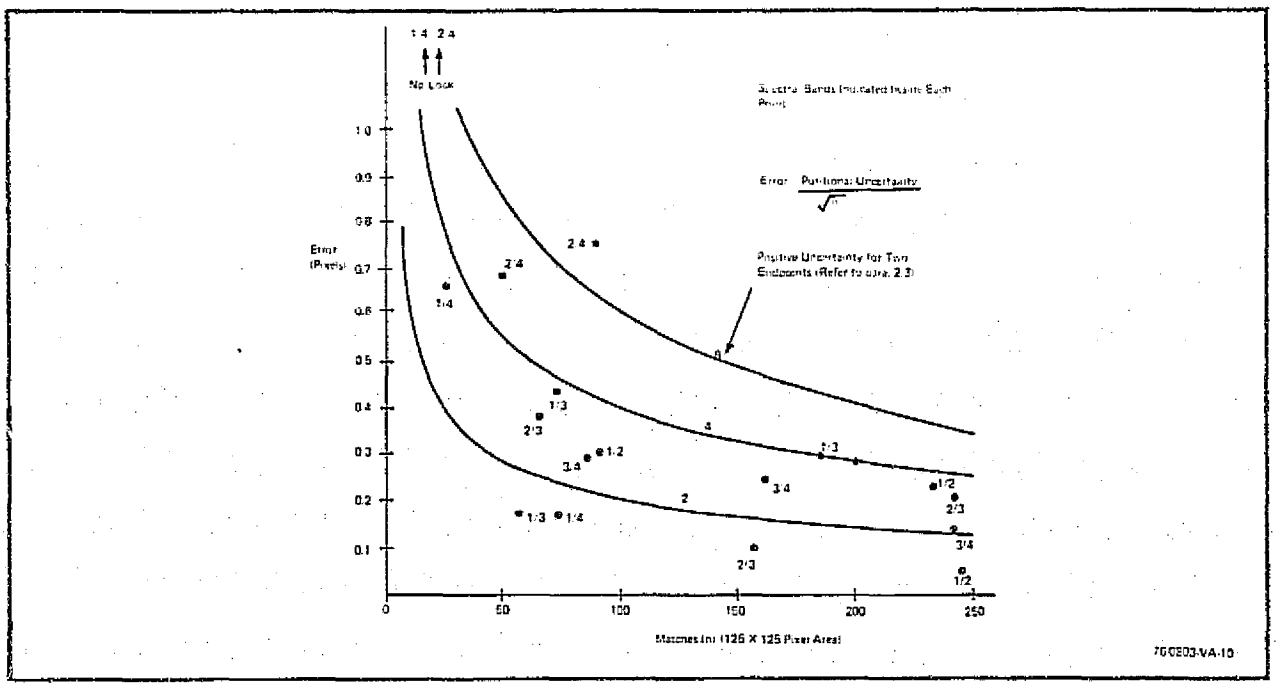

Figure 3-1. Multispectral Registration Error as a Function of the Number of Endpoint Matches in a Window

Also shown are curves that describe the relationship of equation 2-2 for values of positional uncertainty for a pair of endpoints of 2, 4, and 6 pixels. Except for image pairs including band 4, all measurements are within the curve labeled 4. If the assumption is made that the displacement components in Table 3-1 are samples from independent Gaussian distributions and that equation 2-2 holds, then a maximum likelihood estimate of relative positional uncertainty is 3.43 pixels, using all the data. This implies $3.43/\sqrt{2} = 2.43$ pixels positional uncertainty for a single endpoint. If those image pairs that include band 4 are deleted, the estimate of single endpoint uncertainty is 2.05 pixels.

It is noted that the pairs that contain band 4 are frequently high. In fact, in two instances in scene 3, the pairing was so limited that no lock was possible. Loss of lock was also encountered on band 4 for some of the multitemporal measurements (refer to paragraph 3.3).

3.3 Determination of Prefilter and Preprocessor Thresholds

During the processing of the multispectral image pairs, two peculiarities of the LANDSAT image data were observed:

a. A striping effect between adjacent scan lines, evidently caused by uneven sensitivity of the six parallel MSS sensors. The effect is particularly noticeable in uniform areas such as water.

b. A predominance of vertical gradients in the image histograms. Although this could be caused in part by striping between scan lines, an additional cause might be the tighter spacing of data samples in the horizontal direction (along scan) than in the vertical direction (between lines). This discrepancy, due to the MSS scanning format, would accentuate the vertical gradient component.

The above problems should be relieved by prefiltering of the image data. Accordingly, a test was made of the effects of the following filter stages:

1. A smoothing filter that averages all square groups of four pixels in a uniform manner (single-stage square filter)

2. Two stages of the above

3. A filter that averages all vertical groups of two pixels uniformly (vertical, correlation factor K = 1) (vertical refers to the crossing of scan lines)

4. A vertical filter with a correlation factor of 0.4. This value is calculated to correspond to the difference between vertical and horizontal spacing of pixels in the MSS sensor.

In addition, it was desired to establish the importance to the measurements of two preprocessor thresholds, namely:

- The minimum gradient amplitude that would be accepted
- The minimum subset length that would be retained.

The values under consideration for the minimum gradient amplitude were 2 and 3 gray levels (out of 64), and for the minimum subset length, values of 2, 3, and 4 pixels.

Various combinations of these filters and preprocessor parameters were tested on the multitemporal image pair of Figure 2-2, as discussed in paragraph 2.1. The results for relative displacement are shown in Table 3-2 and plotted in Figure 3-2.

The columns in Table 3-2 refer to

a. Type of filter used: One or two sequential stages, using either a square (2 x 2) array, or a comparison between two pixesl arranged vertically

b. Minimum detected gradient amplitude

c. Minimum subset length in pixels

d. MSS spectral band

e. The number of subsets obtained

f. The values for Δx and Δy obtained as described in paragrpah 2.3.1

g. The position of indicated match obtained by linear interpolation

h. The number of matching endpoints.

TABLE 3-2

EFFECTS OF PREFILTERING AND PREPROCESSOR THRESHOLD SELECTION ON THE MEASUREMENTS OF RELATIVE DISPLACEMENT FOR THE WINDOWS IN FIGURE 2-2

Filter	Grad	MSL	Band	Subsets	ΔX	ΔY	Interpolation X	Interpolation Y	Matches
Two-Stage Square	3	3	1	101/69	0.14 - 0.39	0.23 - 0.58	-0 26 - 0.28		57
	3	3	2	114/101	0.23 - 0.25	0.30 - 0.58	-0.48 - 0.34		77
	3	3	3	113/140	-0.03 + 0.35	0.24 - 0.24	+0.08 - 0.50		34
	3	3	4	85/116	No sign change	0.57 - 0.38	–		21
Two-Stage Square	2	3	1	145/100	0.07 - 0.45	0.26 - 0.52	-0.13 - 0.33		87
	2	3	2	162/152	0.26 - 0.22	0 38 - 0.49	-0.54 - 0.44		98
	2	3	3	161/219	-0.14 +0.13	0.41 - 0.10	+0.52 - 0.57		63
	2	3	4	108/165	-0.14 + 0.47	0.65 - 0.22	+0.29 0.75		31
Two-Stage Square	3	2	1	138/92	0.29 - 0.25	0.35 - 0.43	-0.54 - 0.45		83
	3	2	2	157/132	0.31 - 0.20	0.26 - 0.48	-0.61 - 0.35		94
	3	2	3	142/204	No sign change	No sign change	No sign change		53
	3	2	4	113/150	No sign change	0.71 - 0.16	–		31
Two-Stage Square	2	4	1	105/79	0.22 - 0.43	0.32 - 0.48	-0.34 - 0.40		72
	2	4	2	113/112	0.28 - 0.10	0.36 - 0.45	-0.74 - 0.45		61
	2	4	3	115/163	-0.33 + 0.17	0.22 - 0.19	+0.66 - 0.54		45
	2	4	4	82/125	-0.25 + 0.12	0.63 - 0.44	+0.68 - 0.59		24
Two-Stage Square	2	2	1	197/141	0.15 - 0.34	0.21 - 0.62	-0.30 - 0.25		109
	2	2	2	229/210	0.23 - 0.14	0.31 - 0.36	-0.62 - 0.46		137
One-Stage Square	2	3	1	174/129	0.09 - 0.49	0.23 - 0.46	-0.15 - 0.33		91
	2	3	2	203/199	0.02 - 0.44	0.34 - 0.23	-0.04 - 0.59		147
None	2	3	1	273/252	0.30 - 0.[illegible]	.26 - 0.42	-0.51 - 0.38		188
	2	3	2	322/293	0.05 - 0.31	0.38 - 0.34	-0.14 - 0.53		239
One-Stage Vertical K = 0.4	2	3	1	207/179	0.37 - 0.03	0.24 - 0.42	-0.93 - 0.36		131
	2	3	2	221/217	0.16 - 0.30	0.29 - 0.35	-0.35 - 0.45		147
One-Stage Vertical K = 1.0	2	3	1	196/166	0.11 - 0.36	0.05 - 0.44	-0.23 - 0.10		128
	2	3	2	235/222	0.29 - 0.23	0.28 - 0.42	-0.56 - 0.40		167

76-0803-T-11

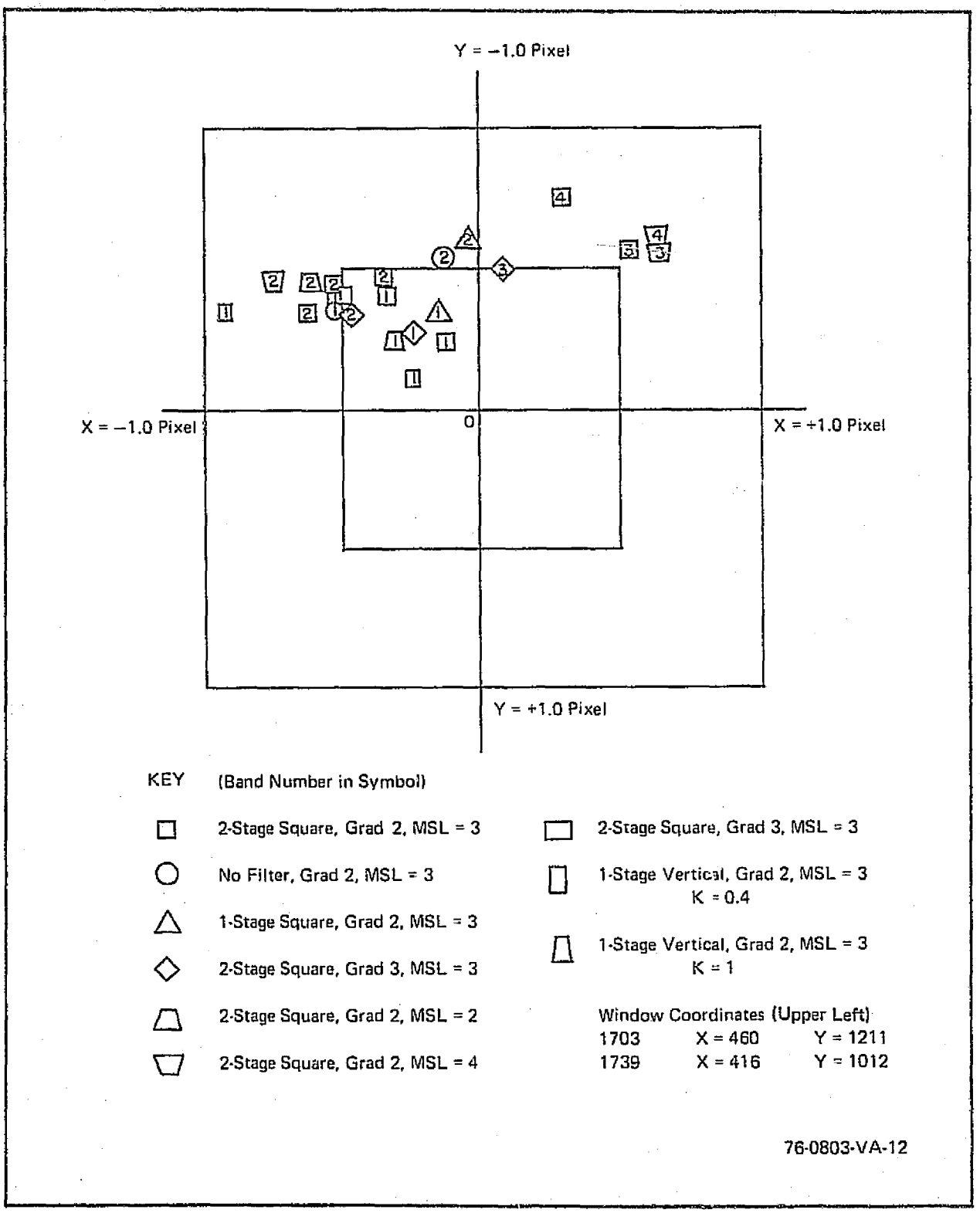

Figure 3-2. Effects of Prefiltering and Preprocessor Threshold Selection on Relative Displacement Measurements for the Windows in Figure 2-2

With reference to Figure 3-2, it is apparent that displacements for bands 3 and 4 are separated from the results for bands 1 and 2 by an average of approximately 0.5 pixel. However, it is noted from Table 3-2 that limited numbers of endpoints were available for these measurements. Although ground truth is not available, the cluster of points for bands 1 and 2 centers at x = -0.39 and y = -0.38. All points for these bands are within half a pixel of this average position. Since the number of available match points is below 100 in half of these measurements, this dispersion is in agreement with the discussion of paragraph 3.2. The effect of the filtering and thresholding on the number of available subsets can be seen in Table 3-2.

The action of the filters in smoothing the gradient histogram is shown in Table 3-3. For each of the filter conditions, the number of gradient samples for the 16 directions (see Figure 2-4) is tabulated. Both band 1 and band 2 are included for both windows of the image pair. For these measurements, a minimum gradient amplitude of 2 was selected, with a minimum subset length of 3.

At the right of Table 3-3, computations were made of the ratio of the number of vertical gradient samples to the number of horizontal samples. The vertical filters clearly perform a smoothing action. In a homogeneous image, one would expect to achieve values approaching unity for these ratios. However, as is evident from Figure 2-5, the horizontal line structure (with vertical gradients) predominates over the vertical structure.

In summary, it was concluded that the choice of a filter and preprocessor thresholds is not critical, provided that sufficient matching endpoints are available. Because it provides smoothing action against sensor striping, as well as the calculated amount of vertical correlation, the vertical filter with a correlation factor of 0.4 was chosen for the later tests. The selected preprocessor thresholds were a minimum gradient amplitude of 2 with a

TABLE 3-3

GRADIENT DIRECTION HISTOGRAMS FOR VARIOUS PREFILTERS FOR WINDOWS IN FIGURE 2-2

		Direction of Gradient Across Edge: Light → Dark				↘		↓		/	←	↖	↑	↗					(R_1) 5/1	(R_2) 13/9	R_1	R_2	$M\ R_1+R_2$
		Grad	MSL	Band	Image	1	2	3	4	5	6	7	8	9	10	11	12	13	14	15	16					
1.	No Filter	2	3	1	1	169	204	250	620	771	625	329	350	170	200	230	484	634	438	338	333	771/169	631/170	4.6	3.7	8.3
2.	One Stage Vert K = 0.4	2	3	1	1	154	224	234	467	539	363	217	418	171	218	215	339	447	330	308	412	539/154	447/171	3.5	2.6	6.1
3.	One-Stage Square	2	3	1	1	105	64	119	459	537	286	249	252	146	99	135	313	399	277	241	308	534/105	399/146	5.1	2.73	7.8
4.	Two-Stage Square	2	3	1	1	55	70	122	432	480	227	232	244	101	72	101	279	337	236	210	253	480/55	337/104	8.7	3.24	11.9
5.	One-Stage Vert. K = 1	2	3	1	1	179	170	233	491	451	322	323	306	171	191	164	329	385	309	254	420	451/179	385/711	2.5	2.2	4.7
6				1	5	138	133	305	404	873	390	416	201	168	175	202	368	626	399	294	297	813/138	620/168	6.3	3.1	9.4
7				1	5	130	218	149	391	133	242	305	406	153	178	177	307	322	264	290	343	433/130	377/153	3.3	2.1	5.4
8	(Same)			1	5	70	49	105	307	429	210	262	249	137	69	106	254	359	262	150	236	429/70	330/137	6.1	2.5	8.6
9				1	5	50	32	73	347	395	140	201	279	104	51	77	230	270	221	141	227	385/50	270/104	7.7	2.6	10.3
10				1	5	136	128	240	375	387	240	345	333	185	132	128	271	319	288	220	329	397/136	319/185	2.9	1.7	4.6
11				2	2	219	258	352	952	915	567	477	467	256	232	282	644	737	639	422	515	915/219	751/256	4.2	2.9	7.1
12				2	2	204	244	240	323	661	388	424	376	246	260	235	412	508	460	313	507	661/204	508/296	3.2	1.7	4.9
13	(Same)			2	2	169	124	159	308	714	371	297	449	174	130	131	305	510	462	331	325	714/157	510/179	4.5	2.9	7.4
14				2	2	103	92	148	521	661	278	270	480	137	98	116	354	403	423	264	307	661/103	403/137	6.4	2.9	9.3
15				2	2	214	221	218	556	647	407	372	516	242	201	202	393	472	447	337	407	647/214	472/242	3.0	2.0	5.0
16				2	6	246	183	356	548	907	467	527	435	211	233	211	476	737	659	401	311	907/245	739/291	3.7	2.5	6.2
17				2	6	262	262	244	495	651	318	412	307	259	299	266	383	512	371	318	465	651/202	512/259	3.2	2.0	5.2
18	(Same)			2	6	147	86	147	486	692	281	346	450	203	109	131	369	513	360	267	355	697/147	513/203	4.7	2.5	7.2
19				2	6	103	77	124	461	620	234	303	460	148	83	113	332	451	353	216	341	620/103	451/148	6.0	3.0	9.0
20				2	6	105	191	288	499	653	327	449	540	256	222	267	363	477	361	345	461	633/195	477/256	3.2	1.9	5.1

76-0803 T-13

minimum subset length of 3. Furthermore, because of limitations on the available number of subsets for this window size, it was decided to perform the remaining tests using bands 1 and 2.

3.4 Measurement of a Distortion Matrix between Multitemporal Images

Following the selection of processor parameters, it was decided to perform relative registration measurements on a regular matrix of positions between two multitemporal images. The images selected were 1703-17590 (Reel 2) and 1739-17575 (Reel 2), as shown in Figure 2-2. The matrix consisted of 16 locations spaced by 200 pixels in both the x and y directions. The upper left corner of the first window of the matrix was located on the NASA tapes as follows:

1703-17590: x = 50
y = 220

1739-17575: x = 6
y = 11

This area corresponds to the mountainous terrain at the top of Figure 2-2.

In accordance with the discussion introducing paragraph 3.2, it was decided to estimate ground truth for these multitemporal images by averaging the measurements for bands 1 and 2. The offset will be identical for each of these multispectral pairs, but the data for each pair should be largely independent. As explained in paragraph 3.3, use of bands 3 and 4 was rejected because of a limited availability of match points. Although conventional correlation techniques might be used as an alternate measurement, its superior reliability is not assured. Visual comparison between image samples could not hope to produce satisfactory results to the precision of a small fraction of a pixel as required here.

Registration measurements for the distortion matrix are contained in Tables 3-4 and 3-5. These tables differ in the choice of the match window size used for the measurements (see Figure 2-11). For the measurements contained in Table 3-4, a match window size of 6 by 6 pixels was used.

TABLE 3-4

MULTITEMPORAL REGISTRATION MEASUREMENTS FOR A MATRIX OF LOCATIONS IN THE IMAGES IN FIGURE 2-2 (MATCH WINDOW 6 x 6 PIXELS)

Location	Band	Subsets	X	ΔX	Y	ΔY	Interpolation X	Interpolation Y	Matches
1	1	392/373	2	-0.07 ± 0.63	6	-0.06 ±0.53	2.10 ± 6.10		290
1/1 2/2	2	400/400	2	-0.02 ± 0.52	6	-0.23 ± 0.49	2.04 ± 6.32		348
2	1	374/362	3	-0.57 ± 0.09	5	-0.56 ± 0.05	3.87 ± 5.92		200
5/5 1/1	2	400/400	3	-0.05 ± 0.19	5	-0.51 ± 0.00	3.74 ± 6.00		335
3	1	288/255	5	-0.10 ± 0.37	5	-0.16 ± 0.61	5.13 ± 5.21		185
9/9	2	400/400	5	-0.23 ± 0.35	5	-0.13 ± 0.51	5.40 ± 5.20		319
4	1	267/209	7	-0.26 ± 0.36	5	-0.09 ± 0.64	7.42 ± 5.12		163
13/13	2	400/400	7	-0.13 ± 0.36	5	-0.04 ± 0.54	7.22 ± 5.07		323
5	1	400/400	0	-0.21 ± 0.24	3	-0.30 ± 0.17	0.47 ± 3.64		256
17/17 18/18	2	400/400	0	-0.30 ± 0.12	3	-0.30 ± 0.22	0.76 ± 3.58		308
6	1	400/358	2	-0.20 ± 0.31	3	-0.17 ± 0.30	2.39 ± 3.36		233
21/21 22/22	2	400/400	2	-0.41 ± 0.26	3	-0.27 ± 0.26	2.61 ± 3.51		337
7	1	400/400	4	-0.11 ± 0.38	3	-0.02 ± 0.48	4.26 ± 3.04		312
25/25 26/26	2	400/400	4	-0.20 ± 0.25	3	-0.15 ± 0.36	4.44 ± 3.29		305
8	1	400/337	5	-0.59 ± 0.04	2	-0.30 ± 0.20	5.93 ± 2.60		250
29/29 30/30	2	400/400	5	-0.53 ± 0.04	2	-0.37 ± 0.08	5.93 ± 3.00		291
9	1	400/400	-1	-0.45 ± 0.06	1	-0.26 ± 0.27	-1 ± 0.88	± 1.49	267
33/33 34/34	2	400/400	-1	-0.37 ± 0.10	1	-0.26 ± 0.38	-1 ± 0.79	± 1.41	276
10	1	400/382	0	-0.53 ± 0.08	1	-0.18 ± 0.22	0.87 ± 1.45		256
37/37	2	400/400	1	-0.20 ± 0.34	1	-0.23 ± 0.23	1.38 ± 1.50		285
11	1	400/392	2	-0.24 ± 0.22	0	-0.47 - 0.01	2.52 ± 0.98		254
41/41 42/42	2	400/400	2	-0.44 ± 0.09	1	-0.02 ± 0.41	2.83 ± 1.05		281
12	1	400/298	4	-0.22 ± 0.14	0	-0.35 ± 0.08	4.61 ± 0.81		183
45/45 46/46	2	400/400	4	-0.27 ± 0.16	0	-0.37 ± 0.14	4.63 ± 0.72		274

76-0803-T-14

TABLE 3-5

MULTITEMPORAL REGISTRATION MEASUREMENTS FOR A MATRIX OF LOCATIONS IN THE IMAGES IN FIGURE 2-2
(MATCH WINDOW 4 x 4 PIXELS)

Location		Band	Subsets	X	ΔX	Y	ΔY	Interpolation X	Interpolation Y	Matches
1	1/1	1	392/373	2	-0.07 + 0.59	6	-0.20 + 0.58	2.11	+ 6.26	248
	2/2	2	400/400	2	-0.08 + 0.53	6	-0.26 + 0.46	2.13	+ 6.36	282
2	5/5	1	374/362	3	-0.43 + 0.15	5	-0.51 + 0.10	3.74	+ 5.84	209
	6/6	2	400/400	3	-0.51 + 0.16	5	-0.61 + 0.07	3.76	+ 5.90	262
3	9/9	1	288/255	5	-0.13 + 0.51	5	-0.12 + 0.67	5.20	+ 5.15	149
	10/10	2	400/400	5	-0.25 + 0.19	5	-0.15 + 0.55	5.57	+ 5.21	253
4	13/13	1	267/209	7	-0.03 + -0.91	5	-0.06 + 0.46	7.07	+ 5.11	134
	10/14	2	400/400	7	-0.13 + 0.54	5	-0.07 + 0.57	7.19	+ 5.11	266
5	17/	1	400/400	0	-0.29 + 0.30	3	-0.37 + 0.15	0.49	+ 3.91	196
	18/	2	400/400	0	-0.37 + -0.13	3	-0.39 + 0.13	0.74	+ 3.75	240
6	21/	1	400/358	2	-0.22 + 0.29	3	-0.21 + 0.38	2.43	+ 3.36	180
	22/	2	400/400	2	-0.42 + 0.24	3	-0.38 + 0.29	2.64	+ 3.57	272
7	25/	1	400/400	4	-0.10 + 0.41	3	-0.04 + 0.52	4.20	+ 3.07	228
	26/	2	400/400	4	-0.23 + 0.26	3	-0.03 + 0.39	4.47	+ 3.07	229
8	29/	1	400/337	5	-0.62 + 0.04	2	-0.43 + 0.17	5.94	+ 2.72	188
	30/	2	400/400	5	-0.51 + 0.07	2	-0.47 + 0.03	5.88	+ 2.94	221
9	33/	1	400/400	-1	-0.48 + 0.16	1	-0.17 + 0.31	-1 + 0.75	+ 1.35	209
	34/	2	400/400	-1	-0.44 + 0.19	1	-0.23 +0.23	-1 + 0.69	+ 1.50	208
10	37/	1	400/382	1	-0.08 + 0.49	1	-0.17 + 0.55	1.14	+ 1.24	189
	38/	2	400/400	1	-0.18 + 0.41	1	-0.19 + 0.27	1.30	+ 1.41	228
11	41/	1	400/392	3	-0.00 + 0.47	0	-0.64 –0.03	3.00	+ 1.00	175
	42/	2	400/400	3	-0.04 + 0.47	1	-0.06 + 0.54	3.08	+ 1.10	207
12	45/	1	400/298	4	-0.34 + 0.20	0	-0.45 + 0.15	4.63	+ 0.75	137
		2	400/400	4	-0.36 + 0.15	0	-0.35 + 0.20	4.71	+ 0.64	210
13	49/	1	400/369	-2	-0.39 + 0.14	-1	-0.25 + 0.30	-2 + 0.74	- 1 + 0.46	209
	50	2	400/400	-2	-0.35 + 0.17	-1	-0.54 + 0.07	-2 + 0.66	- 1 + 0.11	236
14	53/	1	398/274	0	-0.05 + 0.43	-1	-0.21 + 0.51	0 + 0.10	- 1 + 0.29	149
	54/	2	400/400	0	-0.02 + 0.46	-1	-0.35 + 0.20	0 + 0.04	- 1 + 0.64	186
15	57/	1	400/329	1	-0.45 + 0.14	-2	-0.44 + 0.12	1.74	- 2 + 0.79	172
	58/	2	400/400	1	-0.43 + 0.01	-2	-0.32 + 0.14	2.00	- 2 + 0.70	195
16	61	1	400/342	3	-0.29 + 0.01	-2	0.29 + 0.16	3.96	- 2.66	171
	62	2	400/400	3	-0.44 + 0.13	-2	-0.37 + 0.25	3.77	- 2.60	275

76-0803-T-15

For the measurements in Table 3-5, the window size was reduced to 4 x 4 pixels. Reduction of the window size, if otherwise satisfactory, reduces the computational load in the processor for a given image area. Based upon the first 12 measurements, the 4 by 4 match window appeared satisfactory, hence the matrix of 16 positions was completed with the 4 by 4 window alone.

It will be noted in Tables 3-4 and 3-5 that an upper value of 400 subsets occurs on many windows. This value represents the subset storage limitation in the computer simulation program. If this limit is reached in either image, the effective registration area between them is reduced at their lower end. However, the registration accuracy is based on the number of end-points used in the computation; their specific location is not involved.

A display of the array of measurements for the 16-point matrix is shown by Figure 3-3. From these data, it is apparent that a relative orientation and scale difference exists between the images. The rotation is approximately 0.24 degree. The scale difference is 0.9 percent.

Estimation of registration accuracy using these data will be carried out in paragraph 3.7.

3.5 Measurement of a Distortion Matrix between Processed Multitemporal Images

The next tapes received from NASA consisted of Reels No. 2 for images 1062-15190 and 1080-15192 (Chesapeake Bay region). These tapes were understood to be corrected in registration. They each contain a rectangular window of 800 pixels in width by 3200 pixels in height. It was desired to perform registration measurements across the entire length of this image pair.

A series of 24 registration measurements were made on the pair, including comparison measurements for bands 1 (4) and 2 (5) at 12 locations. Four pairs of measurements were made at a separation of 200 pixels at the top of the images; four in the middle and four at the bottom. Data for these measurements are contained in Table 3-6 and plotted in Figure 3-4.

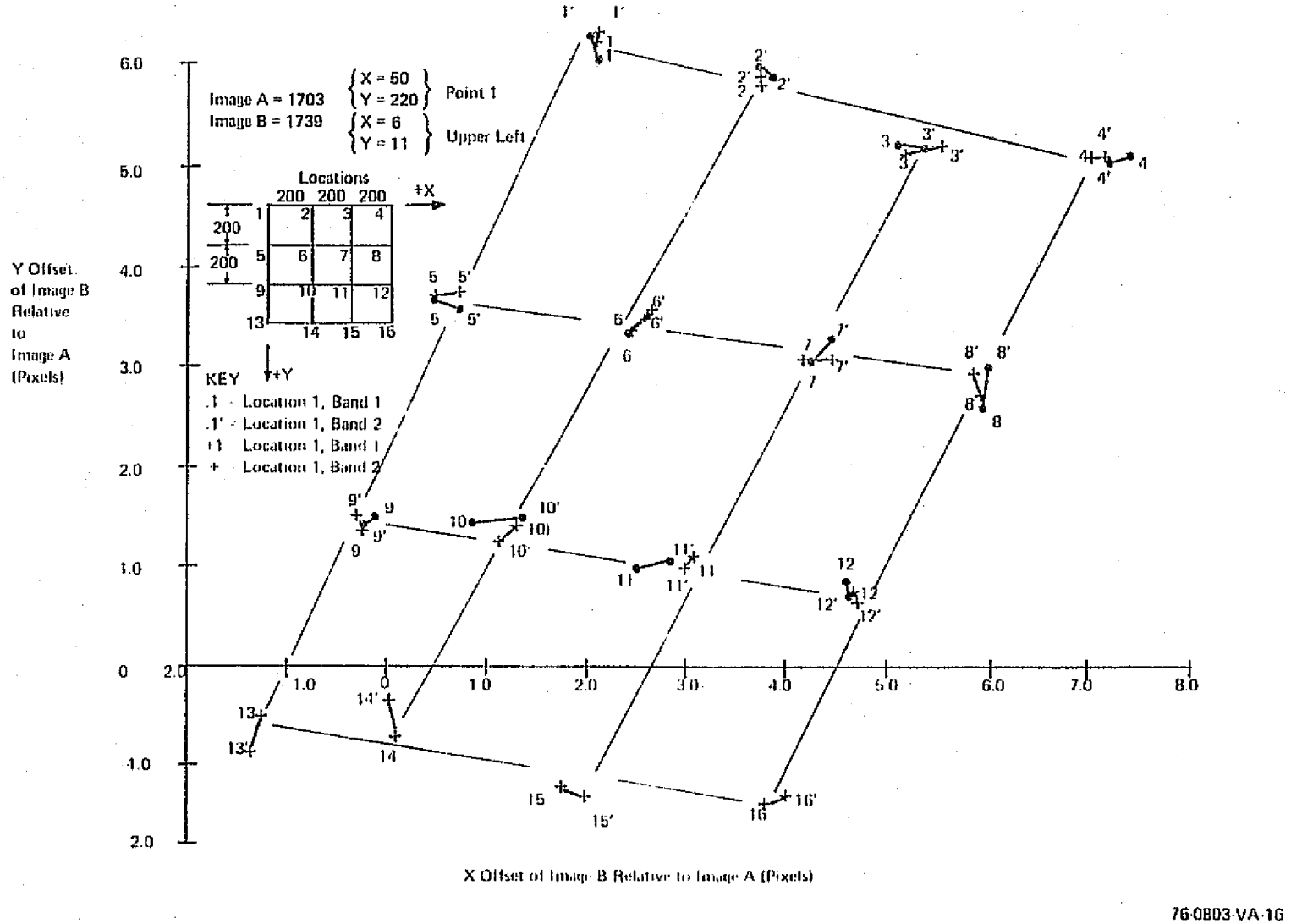

Figure 3-3. Multitemporal Registration Measurements for a Matrix of Locations in the Images in Figure 2-3

TABLE 3-6

MULTITEMPORAL MEASUREMENTS FOR PROCESSED TAPES OF THE CHESAPEAK BAY REGION

Location	Pair	Band	Subsets	X	ΔX	Y	ΔY	Interpolation X	Interpolation Y	Matches
1	1A1B	1	400/324	−1	-0.43 + 0.19	−1	-0.20 + 0.51	-1 + 0.69	-1 + 0.28	172
	2A2B	2	400/400	−1	-0.33 + 0.21	−1	-0.10 + 0.37	-1 + 0.61	-1 + 0.21	228
2	5A5B	1	290/297	−1	-0.56 + 0.23	−1	-0.25 + 0.27	-1 + 0.71	-1 + 0.48	216
	6A6B	2	400/400	−1	-0.46 + 0.27	−1	-0.19 + 0.41	-1 + 0.63	-1 + 0.32	310
3	9A9B	1	307/944	−1	-0.57 + 0.25	−1	-0.41 +0.30	-1 + 0.70	-1 + 0.58	234
	10A10B	2	400/400	−1	0.48 + 0.28	−1	-0.38 + 0.31	-1 + 0.62	-1 + 0.55	318
4	13A13B	1	193/221	−1	-0.46 + 0.39	−1	-0.61 + 0.23	-1 + 0.54	-1 + 0.73	138
	14A14B	2	359/323	−1	-0.50 + 0.31	−1	-0.57 + 0.15	-1 + 0.62	-1 + 0.79	267
5	17A17B	1	247/254	0	-0.15 + 0.63	−1	-0.61 + 0.11	0 + 0.19	-1 + 0.85	202
	18A18B	2	354/329	0	-0.23 + 0.64	−1	-0.40 + 0.31	0 + 0.26	-1 + 0.57	294
6	21	1	251/239	0	-0.20 + 0.74	−1	-0.58 + 0.01	0 + 0.21	-1 + 1.01	159
	22	2	378/305	0	-0.16 + 0.61	−1	-0.60 + 0.15	0 + 0.21	-1 + 0.80	251
7	25	1	322/298	0	-0.09 + 0.66	−1	-0.48 + 0.01	0 + 0.12	-1 + 0.98	203
	26	2	393/377	0	-0.12 + 0.61	−1	-0.48 + 0.15	0 + 0.16	-1 + 0.76	274
8	29	1	400/400	0	-0.11 + 0.60	−1	-0.61 + 0.00	0 + 0.15	-1 + 1.00	343
	30	2	400/400	0	-0.03 + 0.79	−1	-0.60 + 0.10	0 + 0.04	-1 + 0.86	373
9	33	1	81/99	−1	-0.67−0.10	0	-0.19 + 0.40	-1 + 1.18	0 + 0.32	38
	34	2	163/176	−1	-0.60 + 0.13	0	-0.16 + 0.59	-1 + 0.82	0 + 0.21	115
10	37	1	63/76	−1	-0.71 + 0.20	0	-0.58 + 0.10	-1 + 0.78	0 + 0.85	45
	38	2	110/129	−1	-0.69 + 0.14	0	-0.22 + 0.52	-1 + 0.83	0 + 0.31	109
11	41	1	112/196	−1	-0.50 + 0.31	0	-0.32 + 0.32	1 + 0.62	0 + 0.50	88
	42	2	202/278	0	-0.05 + 0.62	0	-0.17 + 0.46	0 + 0.08	0 + 0.27	200
12	45	1	114/184	−1	-0.63 + 0.05	0	-0.10 + 0.63	-1 + 0.94	0 +0.14	101
	46	2	188/240	−1	-0.58 + 0.17	0	-0.03 + 0.69	-1 + 0.77	0 + 0.04	163

76-0803-T-17

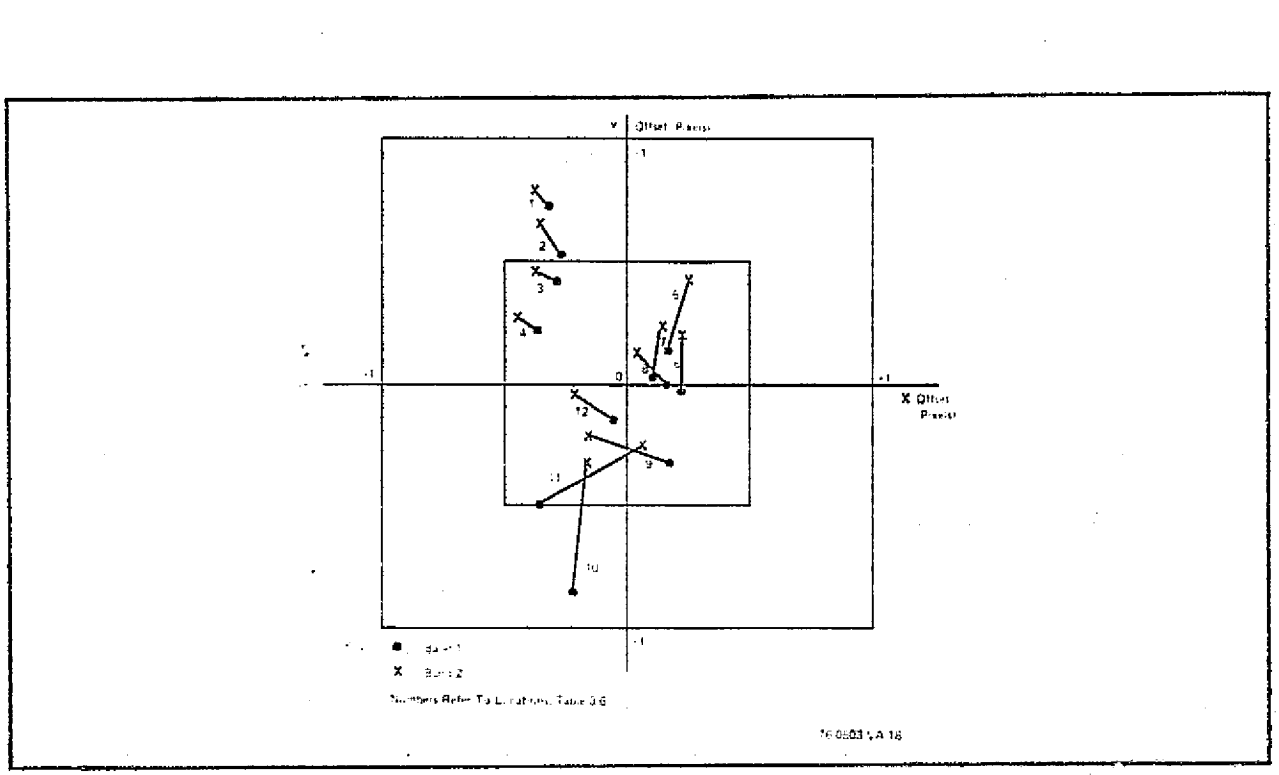

Figure 3-4. Multitemporal Measurements for Processed Tapes of the Chesapeake Bay Region

It is evident that the distortion between these images is less than 1 pixel. However, based upon the clustering of the measurements for top, middle, and bottom, a warping to the right exists in the middle of image B relative to image A.

It is of interest that the selection of the measurement matrix did not involve prior examination of the image areas.

3.6 Quality Measurements on Specially Processed Multitemporal Images

This series of measurements is a quality determination of an attempt to insert a window of image 1739 into image 1703 (see Figure 2-2). The coordinates of the insert in image 1703 are shown in Figure 3-5, along with the results obtained. The data are contained in Table 3-7. For this test only image data for band 2 (5) were supplied.

The data of Figure 3-5 show that at the top of the insert its position is lowered relative to 1703 (y is positive), while at the bottom, it is raised (y is negative). In effect, the insert is compressed by nearly 3 pixels in the vertical direction.

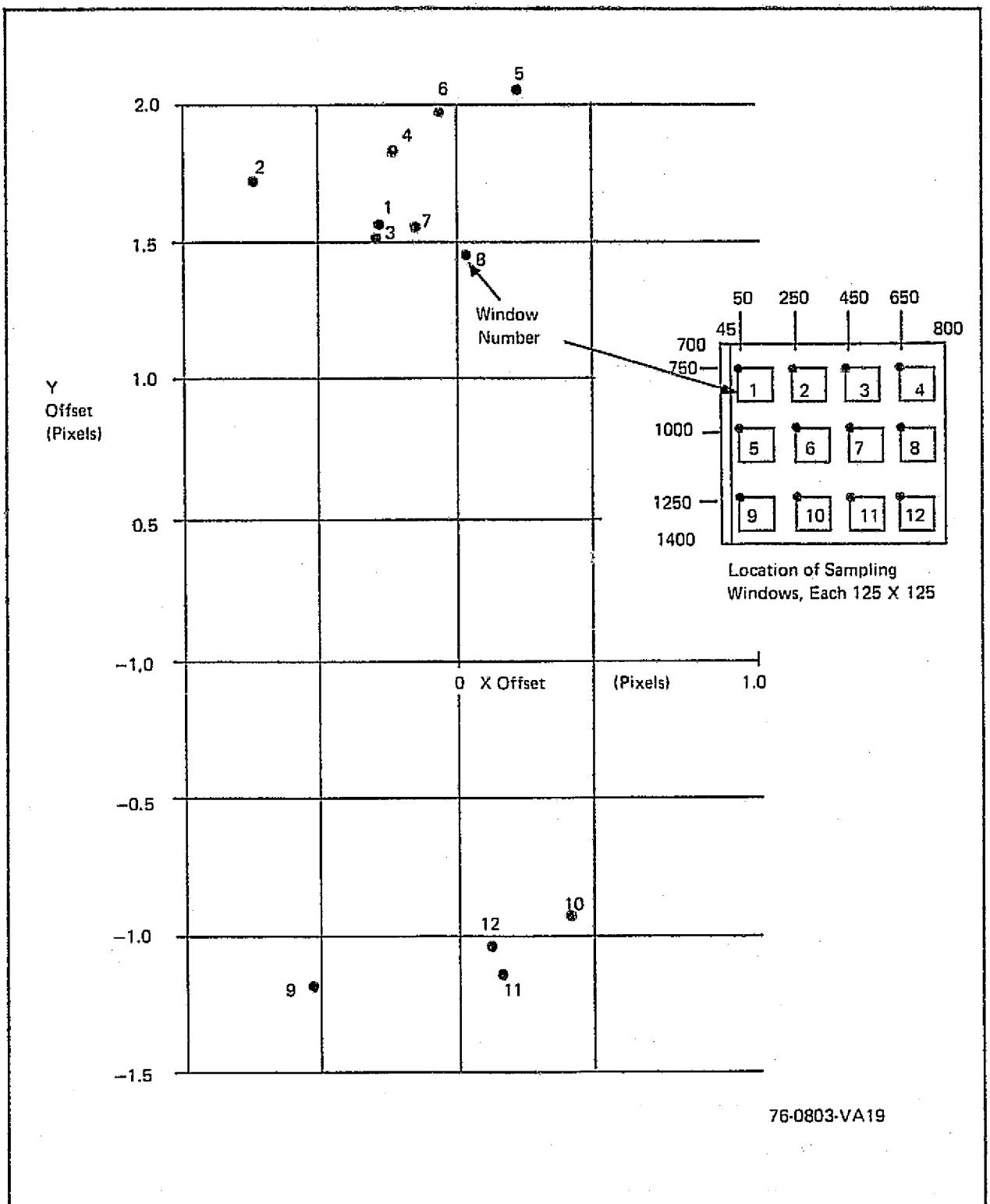

Figure 3-5. Quality Measurements on Processed Multitemporal Images

TABLE 3-7

QUALITY MEASUREMENTS ON PROCESSED MULTITEMPORAL IMAGES

Window Number & Location	Subsets	X	ΔX	Y	ΔX	Interpolaton X	Interpolaton Y	Matches
1 50,750	400/400	−1	-0.41 +0.17	1	-0.39 + 0.31	-1 +0.72	1 +0.56	180
2 250,750	400/400	−1	-0.08 + 0.22	1	-0.34 + 0.14	-1 + 0.27	1 + 0.71	199
3 450,750	400/400	−1	-0.42 + 0.16	1	-0.30 + 0.28	-1 + 0.72	1 + 0.52	191
4 650,750	400/400	−1	-0.36 +0.10	1	-0.42 +0.09	-1 + 0.78	1 + 0.82	223
5 50,1000	298/349	0	-0.11 + 0.35	2	-0.01 + 0.44	0 + 0.24	2 + 0.02	142
6 250,1000	400/400	−1	-0.47 + 0.03	1	-0.54 + -0.01	-1 +0.92	1 + 0.98	204
7 450,1000	400/400	−1	-0.43 + 0.08	1	-0.30 + 0.25	-1 +0.84	1 + 0.55	239
8 650,1000	400/400	0	-0.55 + 0.01	1	-0.21 + 0.26	0 +0.02	1 + 0.45	237
9 50,1250	291/400	−1	-0.17 + 0.18	−2	-0.42 + 0.10	-1 +0.49	-2 + 0.81	159
10 250,1250	225/256	0	-0.23 + 0.29	−1	-0.02 + 0.35	0 +0.44	-1 + 0.05	135
11 450,1250	208/237	0	-0.08 + 0.39	−2	-0.53 + 0.10	0 + 0.17	-2 + 0.84	143
12 650,1250	320/295	0	-0.04 + 0.25	−2	-0.60 + 0.03	0 + 0.14	-2 + 0.95	188

76-0803-T-20

3.7 Estimate of Registration Accuracy

Determination of registration accuracy is based upon a comparison with ground truth. As explained in paragraph 3.4, an estimate of ground truth is made for the multitemporal images by averaging measurements for bands 1 and 2. Table 3-8 includes a collection of difference components (Δx, Δy) for the measurements of bands 1 and 2 from Tables 3-4, 3-5, and 3-6. From these components, the magnitude of the radial registration error for either band alone is

$$\Delta = \sqrt{\frac{(\Delta x)^2 + (\Delta y)^2}{2}} \qquad (3\text{-}1)$$

This formula assumes that the measured difference between the two displacement vectors at a given location results from combining two error vectors having a random angular relationship. In accordance with equation 2-3, an estimate for the value of one of them would be the value for Δ shown by equation 3-1.

In addition to the computed values for Δ, Table 3-8 indicates the number of matching endpoint pairs obtained for both band 1 and band 2 in each case.

At the bottom of Table 3-8 are shown the mean errors $\overline{\Delta}$, for each set of measurements and for the group as a whole. The rms value, Δ_{rms}, is also computed. In accordance with previous comment, Δ_{rms} is the maximum likelihood estimate of the radial registration error.

A histogram of these error measurements is shown by Figure 3-6, including the location of the average and rms error values. The following comments seem appropriate with respect to these results:

a. None of the estimated errors exceeds 0.45 pixel

b. Both the average and rms values of the error are less than 0.20 pixel

c. Two of the three estimates above 0.30 pixel are based on limited numbers of matching endpoints (fewer than 100).

TABLE 3-8

ERROR COMPUTATIONS FROM EARLIER REGISTRATION MEASUREMENTS

Location	From Table 3-4				From Table 3-5				From Table 3-6			
	ΔX	ΔY	Δ	Matches	ΔX	ΔY	Δ	Matches	ΔX	ΔY	Δ	Matches
1	0.06	0.22	0.16	290/348	0.02	0.10	0.07	248/282	0.08	0.07	0.07	172/228
2	0.13	0.08	0.11	280/335	0.02	0.06	0.04	209/262	0.08	0.16	0.13	216/310
3	0.27	0.01	0.19	185/319	0.37	0.06	0.27	149/253	0.08	0.03	0.06	234/318
4	0.22	0.05	0.14	163/323	0.12	0	0.08	134/266	0.08	0.06	0.07	136/267
5	0.29	0.06	0.21	256/308	0.25	0.04	0.18	196/240	0.07	0.28	0.20	202/294
6	0.22	0.15	0.19	233/337	0.21	0.21	0.21	180/272	0	0.21	0.15	159/251
7	0.18	0.25	0.22	312/305	0.27	0	0.19	228/229	0.02	0.22	0.16	203/274
8	0	0.40	0.28	250/291	0.06	0.22	0.16	188/221	0.12	0.14	0.13	343/373
9	0.09	0.08	0.09	267/276	0.06	0.15	0.11	209/208	0.36	0.11	0.27	38/115
10	0.51	0.05	0.36	256/285	0.16	0.17	0.17	189/228	0.05	0.54	0.38	45/109
11	0.31	0.07	0.22	254/281	0.08	0.10	0.09	175/207	0.59	0.23	0.45	88/200
12	0.02	0.09	0.07	183/274	0.08	0.11	0.10	137/210	0.17	0.10	0.14	101/163
13					0.08	0.35	0.25	209/236				
14					0.06	0.35	0.25	149/186				
15					0.26	0.09	0.19	172/195				
16					0.19	0.06	0.14	171/225				
$\overline{\Delta}$			0.185				0.156				0.184	
Δ rms			0.201				0.169				0.218	

Overall : $\overline{\Delta}$ 0.173

Δ rms 0.195

76-0803-T-21

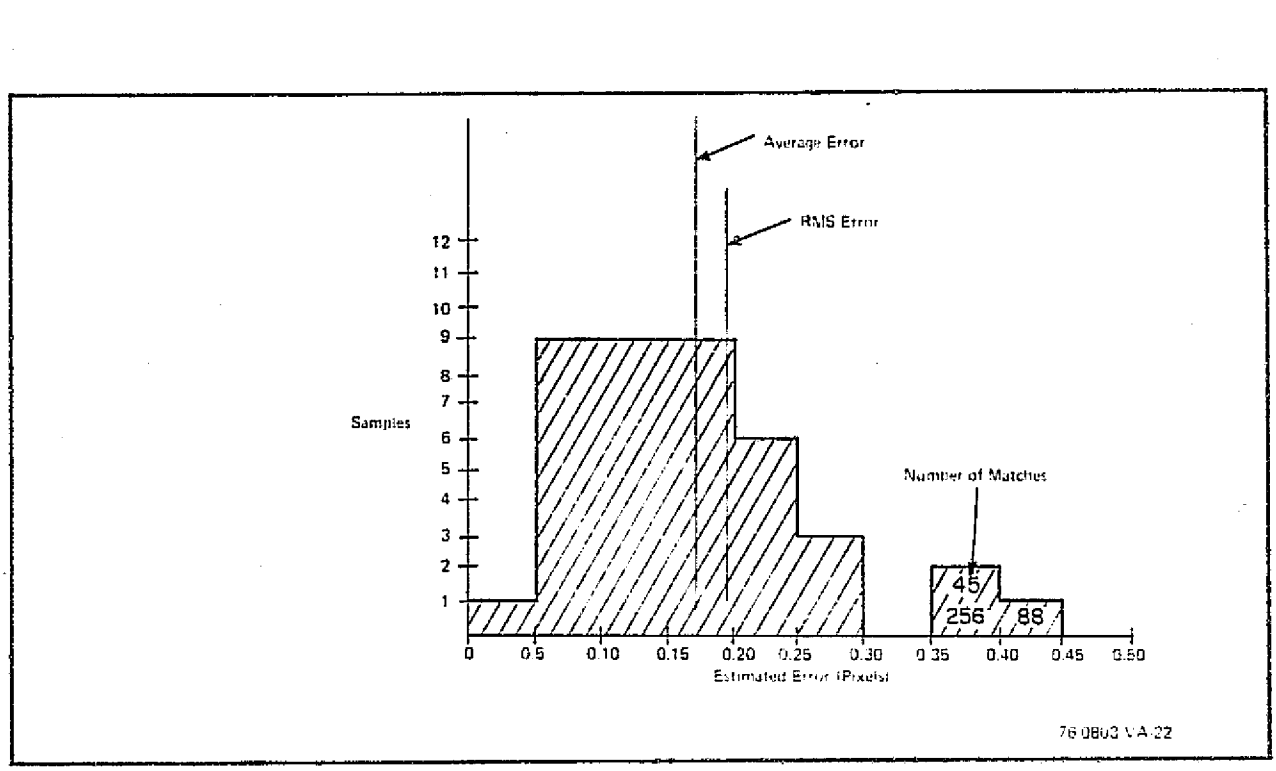

Figure 3-6. Histogram of Estimated Error for 40 Measurements

d. The registration measurements were made in accordance with a fixed positional matrix. No attempt was made to choose matching areas.

e. It should be noted that the data from Tables 3-4 and 3-5 are correlated to the extent that the same preprocessor outputs were used for locations 1-12. However, a different matching window size was used (6 by 6 for Table 3-4, 4 by 4 for Table 3-5).

Figure 4-1. View of Westinghouse Pattern Recognition Laboratory showing the Breadboard Digital Image Processor

devices, video tape recording equipment, and test instrumentation. A console on the bench at right supplies the minicomputer program via punched paper tape. A configuration of this kind could be programmed to perform registration operations.

4.2 Programmable Processor (General-Purpose Computer)

The output of the preprocessor (subsets) will be fed directly to a buffer associated with the programmable processor. The processor must then accomplish the following functions:

1. Binning of subsets in accordance with the registration window format

2. Generation of a search array from the stored subsets of the reference window.

3. Proximity search of subset endpoints from the incoming window with respect to the reference window

4. Check of matching subset endpoints

5. Computation of indicated and relative displacements.

The computation of displacements is a relatively minor portion of the computer load. Consequently, search operations for up to 10 pixels around a given point can easily be accommodated. Initial acquisition should be possible between LANDSAT images on this basis.

The specific determination of pixel throughput rates will depend on a detailed examination of processor characteristics and the determination of the data format, including desired accuracy, spacing of registration windows, and image dimensions. However, it is proposed to select a specific set of operating conditions so as to provide an indication of the system capability. If we assume an image width of 200 pixels, of any length, and with registration windows spaced 200 pixels apart both across and down, then at a 1-megapixel-per-second processing rate, a set of four windows will be processed every 0.16 second. If it is further assumed that 200 subsets (400 endpoints) will be available, on the average, in each window and that 150 matches will be obtained per window, then the number of equivalent add operations required by the processor will be approximately 150,000. If the processor add time is 1 microsecond, the processor will complete the required computations in 0.15 second, or slightly ahead of the available 0.16 second. Accuracy will be in the neighborhood of 0.3 pixel. Initial acquisition will be possible as well as continued registration.

Tradeoffs on the above example can be made with regard to accuracy, processing speed, and the size and capability of the general-purpose processor. As explained in paragraph 2.3, accuracies approaching 0.1 pixel should be obtained by increasing the level of matches to 800 (a factor of 5). The processing load would be increased under these conditions by a corresponding amount.

5. CONCLUSIONS AND RECOMMENDATIONS

It is concluded that the primary objectives of this program have been met. The Westinghouse registration techniques appear capable of performing on LANDSAT images, on either a multispectral or multitemporal basis, to accuracies of a small fraction of a pixel. They are insensitive to the choice of registration area, provided terrain detail is available, which suggests application to automated systems. They may be implemented at megapixel-per-second rates, using commercial minicomputers in combination with a special-purpose preprocessor. In this configuration, they could find application as a rapid means for assessing image geometric quality.

5.1 Conclusions

More detailed conclusions are as follows:

a. Reasonable agreement was found between the estimated accuracy (paragraph 2.3) and the measured accuracy, both multispectral (paragraph 3.2) and multitemporal (paragraph 3.7).

b. The highest value of estimated registration error was 0.45 pixel. For a series of 40 measurements, both the mean radial error and rms radial error were less than 0.20 pixel (paragraph 3.7).

c. An indication of measurement quality is given by the number of matches involved in the computation (paragraph 2.3).

d. Accuracy to 0.1 pixel could be expected by increasing the registration window size.

5.2 Recommendations

The following recommendations are made:

a. For implementation of these registration techniques as a quality control tool, a brief study of the desired system configuration should be made, including the available general-purpose processor, image formats, and speed and accuracy requirements. Acquisition of a preprocessor should be considered.

b. Additional statistical data collection might be of interest, to include:

1. Effects of cloud cover
2. Effects of water areas
3. Additional examination of performance with bands 3 and 4
4. Measurements to establish accuracy to 0.1 pixel.